AGU ADVANCING EARTH AND SPACE SCIENCE

Earth and Space Science

RESEARCH ARTICLE
10.1029/2022EA002694

**Key Points:**

- Visible to near-infrared spectra of (16) Psyche are consistent with meteorites (irons and metal-rich chondrites) and sulfides
- The Psyche mission's Multispectral Imager can identify and potentially discriminate such materials if present on the surface of Psyche
- Imager-convolved data indicate that the instrument can accurately recover absorption band parameters in certain metal-silicate mixtures

**Supporting Information:**

Supporting Information may be found in the online version of this article.

**Correspondence to:**

S. D. Dibb,
dibb@baeri.org

**Citation:**

Dibb, S. D., Bell, J. F., III, Elkins-Tanton, L. T., & Williams, D. A. (2023). Visible to near-infrared reflectance spectroscopy of asteroid (16) Psyche: Implications for the Psyche mission's science investigations. *Earth and Space Science*, *10*, e2022EA002694. https://doi.org/10.1029/2022EA002694

Received 27 OCT 2022
Accepted 23 DEC 2022

**Author Contributions:**

**Conceptualization:** S. D. Dibb, J. F. Bell III, L. T. Elkins-Tanton, D. A. Williams
**Data curation:** S. D. Dibb, J. F. Bell III
**Formal analysis:** S. D. Dibb
**Funding acquisition:** J. F. Bell III, L. T. Elkins-Tanton, D. A. Williams
**Investigation:** S. D. Dibb, J. F. Bell III, L. T. Elkins-Tanton, D. A. Williams
**Methodology:** S. D. Dibb, J. F. Bell III



# Visible to Near-Infrared Reflectance Spectroscopy of Asteroid (16) Psyche: Implications for the Psyche Mission's Science Investigations

**S. D. Dibb[1,2], J. F. Bell III[2], L. T. Elkins-Tanton[2], and D. A. Williams[2]**

[1]Bay Area Environmental Research Institute, NASA Ames Research Center, Moffett Field, CA, USA, [2]School of Earth and Space Exploration, Arizona State University, Tempe, AZ, USA

**Abstract** The NASA Psyche mission will explore the structure, composition, and other properties of asteroid (16) Psyche to test hypotheses about its formation. Variations in radar reflectivity, density, thermal inertia, and visible to near-infrared (VNIR) reflectance spectra of Psyche suggest a highly metallic composition with mafic silicate minerals (e.g., pyroxene) heterogeneously distributed on the surface in low abundance (<10 vol.%). The Psyche spacecraft's Multispectral Imager is designed to map ≥80% of the surface at high spatial resolution (≤20 m/pixel) through a panchromatic filter and provide compositional information for about ≥80% of the surface using seven narrowband filters at VNIR wavelengths (~400–1,100 nm) and at spatial scales of ≤500 m/pixel. We analyzed 359 reflectance spectra from samples consistent with current uncertainties in Psyche's composition and compared them to published reflectance spectra of the asteroid using a chi-square test for goodness of fit. The best matches for Psyche include iron meteorite powder, powders from the sulfide minerals troilite and pentlandite, and powder from the CH/CBb chondrite Isheyevo. Comparison of absorption features support the interpretation that Psyche's surface is a metal-silicate mixture, although the exact abundance and chemistry of the silicate component remains poorly constrained. We convolve our spectra to the Imager's spectral throughput to demonstrate preliminary strategies for mapping the surface composition of the asteroid using filter ratios and reconstructed band parameters. Our results provide predictions of the kinds of surface compositional information that the Psyche mission could reveal on the solar system's largest M-type asteroid.

**Plain Language Summary** Current observations of the asteroid (16) Psyche suggest it to be metal-rich, but not entirely made of metal. We compared reflected light from a wide variety of Psyche-relevant materials to measurements of reflected light from the asteroid. This analysis confirms that Psyche's composition could be less metal-rich than previously thought. Other materials with reflectance properties similar to Psyche are metal-rich carbonaceous chondrites and sulfide minerals. We show how an instrument on the Psyche spacecraft, which will study the asteroid in detail, can resolve some uncertainties about the surface composition of the asteroid.

## 1. Introduction

Asteroid (16) Psyche is the largest of the M-type asteroids and is the target of the NASA Psyche mission (Elkins-Tanton et al., 2020). Within the last few decades, multiple studies have observed the surface of Psyche at ultraviolet to infrared wavelengths and have generally interpreted the surface to be dominated by Fe-Ni metal with a minor (<10 vol.%) component of low-Fe, low-Ca pyroxene (e.g., DeMeo et al., 2009; Fornasier et al., 2010; Hardersen et al., 2005; Ockert-Bell et al., 2010). Since NASA's selection of the Psyche mission in early 2017, there has been renewed interest in visible to near-infrared (VNIR) spectroscopic study and interpretation of the asteroid's surface mineralogy (e.g., Becker et al., 2020; Cantillo et al., 2021; Dibb et al., 2022; Sanchez et al., 2017; Takir et al., 2017). In addition to spectroscopic observations, density estimates and measurements of both radar reflectivity and thermal inertia of Psyche are consistent with the presence of core-like materials, such as iron meteorites and sulfide minerals like troilite (FeS) (Cambioni et al., 2022; de Kleer et al., 2021; Elkins-Tanton et al., 2020; Landsman et al., 2018; Matter et al., 2013; Shepard et al., 2021; Siltala & Granvik, 2021).

A synthesis of observations of Psyche indicates that plausible bulk compositions could be far less metallic (~30–55 vol.% metal) than previously thought, with significant pore space and a still unknown non-metal component (Elkins-Tanton et al., 2020, 2022). New studies since selection do not alter the mission's primary

**Project Administration:** J. F. Bell III, L. T. Elkins-Tanton
**Resources:** J. F. Bell III, L. T. Elkins-Tanton
**Software:** S. D. Dibb
**Supervision:** S. D. Dibb, J. F. Bell III, L. T. Elkins-Tanton, D. A. Williams
**Validation:** S. D. Dibb, J. F. Bell III, L. T. Elkins-Tanton, D. A. Williams
**Visualization:** S. D. Dibb
**Writing – original draft:** S. D. Dibb
**Writing – review & editing:** S. D. Dibb, J. F. Bell III, L. T. Elkins-Tanton, D. A. Williams

hypothesis, which is that the asteroid is a remnant core of a differentiated planetesimal that had its silicate mantle mostly stripped in a series of hit-and-run style collisions (e.g., Asphaug, 2010; Asphaug & Reufer, 2014; Sarid et al., 2015). Other hypotheses for the formation of Psyche include the reaccretion of mostly core materials from a catastrophically disrupted planetesimal, or preservation of a primitive, undifferentiated body with high metal content (Elkins-Tanton et al., 2022). If Psyche indeed contains materials from a planetesimal core, it offers an unparalleled opportunity to explore the nature and evolution of planetary interiors. Data returned from the mission will offer strong constraints on models of solar system evolution and greatly inform our understanding of terrestrial planet formation.

To test these hypotheses, the Psyche spacecraft will be equipped with a set of science instruments that includes the Psyche Multispectral Imager system (henceforth called the "Imager"; Bell et al., 2016; Elkins-Tanton et al., 2022). The Imager is equipped with one broadband and seven narrowband science filters at visible to near-infrared wavelengths (~400–1,100 nm) chosen to study the asteroid's surface geology, composition, and topography (Table 1; Bell et al., 2016; Dibb et al., 2018). The spacecraft's Gamma Ray and Neutron Spectrometer (GRNS) will measure the elemental composition of Psyche's surface at high energy resolution but relatively low spatial resolution, while the Imager will acquire high spatial resolution (~20 m/pixel) information about the asteroid's surface mineralogy. Planned mapping orbits at 704, 293, 174, and 71 km average altitude correspond to estimated ideal pixel scales of approximately 35, 15, 9, and 4 m/px, respectively, for imaging with the broadband filter. Integration of data from the Imager and GRNS will be critical for understanding the surface composition of Psyche.

## 2. Materials and Methods

### 2.1. Natural and Synthetic Laboratory Samples and Mixtures

To support future interpretation of Imager data, we compiled a library of 359 reflectance spectra from possible analog materials that fall within the range of expected Psyche surface minerals, given the hypotheses and uncertainties surrounding the asteroid's origin (Elkins-Tanton et al., 2020, 2022). These materials include a variety of meteorites (irons, pallasites, mesosiderites, CB chondrites, ordinary and enstatite chondrites, aubrites, a diogenite and lodranite, and anomalous, ungrouped metal-rich chondrites). We include spectra from sulfide minerals (troilite (FeS), pyrrhotite ($Fe_{1-x}S$), pentlandite ($(Fe,Ni)_9S_8$), oldhamite (CaS), and a mixture of chalcopyrite ($CuFeS_2$) and pentlandite) and mixtures of iron meteorite metal and troilite (Dibb et al., 2021, 2022). We also included spectra of iron meteorites, enstatite chondrites, mixtures of silicate minerals, and mixtures of silicates and iron meteorite powder from the University of Winnipeg Planetary Spectroscopy Facility (Cloutis et al., 2009, 2010; Horgan et al., 2014; Izawa et al., 2010). We included reflectance spectra from the NASA RELAB Facility at Brown University database of synthetic olivine and pyroxene of a variety of compositions in anticipation of areas of differing silicate chemistry or abundance (Dyar et al., 2009; Klima et al., 2007). Finally, we included additional spectra of synthetic and natural sulfide minerals from the RELAB database to account for differences in spectra of natural and synthetic sulfides (e.g., Helbert et al., 2013; Varatharajan et al., 2019).

### 2.2. Sample Preparation and Measurements

The comparison of laboratory spectral data to telescopic spectral data is highly dependent on properties of both the measurement (primarily phase angle between the incident light source and detector but also ambient lab conditions like temperature and humidity) and the sample (composition and grain size or surface roughness). An informed comparison of laboratory and telescopic data requires documentation of these properties, especially for spectral data from public sources. The source, name, physical form and properties (e.g., hand sample, powder, slab), mineralogy, and measurement phase angle of the spectra in our library are shown in Table S1.

For spectral data collected at Arizona State University, we collected visible to near-infrared (350–2,500 nm) reflectance spectra from samples loaned from the ASU Buseck Center for Meteorite Studies. Spectra were measured using an ASD FieldSpec 4 Standard-Res spectroradiometer. The spectral sampling of this instrument is 1 nm, while the spectral resolution is 3 nm in the visible to near-infrared (350–1,000 nm) and 10 nm in the shortwave infrared (1,000–2,500 nm). Spectra were measured relative to a Spectralon white reference target in air at a phase angle of 30°. We measured spectra of strongly specularly reflecting samples at an incidence angle of 38° and emission angle of 8° to avoid stray light artifacts from the order-sorting filter in the FieldSpec 4 instrument.

**Table 1**
*Psyche Imager Bandpasses*

| # | ECAS name[a] | Center wvl. (nm) | Effective center[b] (nm) | FWHM[c] (nm) | Justification |
|---|---|---|---|---|---|
| 0 | -- | -- | -- | -- | ND5 "Sun safe" blocking filter |
| 1 | CLR | 540 | 516 | 280 | Unfiltered CCD for OpNav, topography, and geology |
| 2 | b | 437 | 442 | 50 | Sulfide detection and blue component of true color |
| 3 | o | 495 | 498 | 25 | Sulfide detection |
| 4 | v | 550 | 553 | 25 | Sulfide detection and green component of true color |
| 5 | w | 725 | 727 | 40 | Typical peak reflectance continuum and red component of true color |
| 6 | x | 850 | 850 | 50 | Search for Fe-bearing silicates and other 1,000 nm features |
| 7 | p | 948 | 946 | 50 | Search for Fe-bearing silicates and other 1,000 nm features |
| 8 | z | 1,041 | 1,015 | 90 | Search for Fe-bearing silicates and other 1,000 nm features |

[a]Filter names that are comparable to those from the Eight Color Asteroid Survey (Zellner et al., 1985). [b]Effective centers are computed after convolution of each bandpass with Imager quantum efficiency, solar emission, and representative spectra of Psyche. [c]Full width at half maximum.

This has negligible impact on reflectance, spectral slope, or band parameters. For some samples, spectra were collected at additional phase angles of 15° and 45° to explore trends in spectral parameters with phase angles. For hand samples, slabs, and gravels, we created average spectra representative of the bulk sample by rastering across the available surface of each sample, given that the surface was visibly free of weathering, oxidation, or other contamination.

Several meteorites and minerals in the ASU collection were powdered as part of research to support spectral interpretations of metal-rich asteroids (e.g., Dibb et al., 2021, 2022). These include sulfide minerals, iron meteorites, and a piece of the metal-rich CH/CBb chondrite Isheyevo. Details for the production and verification of powder from these samples is given by Dibb et al. (2021, 2022). In summary, two iron meteorites (Gibeon and Sikhote-Alin) were manually ground with diamond-coated files, while the sulfides and the piece of Isheyevo were comminuted in a stainless steel impact mortar and pestle. The contents of the powders were examined for contamination both under a microscope and using powder X-ray diffraction, which both indicated minimal contamination (Dibb et al., 2022). Spectra were collected from unsorted powders (i.e., all grains less than ∼1 cm) and from <75 μm to >75 μm sieved fractions. This grain size is consistent with hypothesized grain sizes of the surface of (16) Psyche (e.g., Landsman et al., 2018). Spectra of powder samples were measured with the powder in an aluminum sample cup. We rotated the sample cup at 90° increments, collecting spectra through a full rotation. We then emptied the powder onto clean weighing paper before repeating the process, then averaged all spectra to create a representative bulk spectrum.

### 2.3. Visible to Near-Infrared Telescopic Spectral Data of (16) Psyche

Table 2 lists studies within the past several decades that have collected spectral data of Psyche at visible to near-infrared wavelengths (e.g., DeMeo et al., 2009; Fornasier et al., 2010; Hardersen et al., 2005; Ockert-Bell et al., 2008; Sanchez et al., 2017). These data show that the spectrum of Psyche is red-sloped and relatively featureless, with a subtle absorption feature at ∼1,000 nm. This feature is interpreted as being caused by a relatively

**Table 2**
*Spectral Measurements and Properties of (16) Psyche*

| Study | Observation date (UTC time) | Solar phase angle (°) | Wvl. range (nm) | Visual albedo | Band 1 center (nm) | Band 1 depth (%) |
|---|---|---|---|---|---|---|
| SMASS/DeMeo et al. (2009) | 2000 October 09 | 13.35[a] | 435–2,500[b] | n.r. | n.r. | n.r. |
| Ockert-Bell et al. (2010) | 2005 November 15 | 9.9, 10.2 | 435–3,000[b] | 0.19 | 950 ± 10 | 0.015 ± 0.003 |
| Fornasier et al. (2010) | 2004 November 15 (19:31) | 22.13[a] | 400–2,400 | 0.12 | 949 ± 8 | 2.9 |
| Hardersen et al. (2005, 2011) | 2002 March 22 | 7.12 | 750–2,500 | 0.1203 | 932 ± 8 | ∼1 |
| Sanchez et al. (2017) | 2015 December 08 (10:30) | 1.8 | 690–2,500 | n.r. | 940 ± 10 | 1.3 ± 0.1 |
| | 2015 December 08 (11:43) | 1.8 | 690–2,500 | n.r. | 940 ± 5 | 1.4 ± 0.1 |
| | 2015 December 08 (12:47) | 1.8 | 690–2,500 | n.r. | 935 ± 10 | 1.0 ± 0.1 |
| | 2015 December 09 (14:01) | 1.7 | 690–2,500 | n.r. | 940 ± 3 | 1.2 ± 0.1 |
| | 2016 February 10 (5:10) | 19.5 | 690–2,500 | n.r. | 935 ± 4 | 1.3 ± 0.1 |
| | 2016 February 10 (5:30) | 19.5 | 690–2,500 | n.r. | 919 ± 6 | 1.0 ± 0.1 |
| | 2016 February 10 (6:34) | 19.5 | 690–2,500 | n.r. | 919 ± 3 | 1.3 ± 0.1 |
| | 2016 February 10 (8:05) | 19.5 | 690–2,500 | n.r. | 928 ± 6 | 1.5 ± 0.1 |

[a]Not reported (n.r.) but determined based on reported observation date using the JPL HORIZONS tool. [b]Used data from the SMASS II data set (Bus & Binzel, 2002).

low abundance of low-Fe, low-Ca orthopyroxene (i.e., enstatite). Uncertainties on reported band centers allow possible band centers between ∼913 and ∼960 nm and band depths ranging from ∼0% to 2.9%.

Studies of the variation in pyroxene band center with changes in pyroxene chemistry suggest that the chemistry of the purported pyroxene on Psyche could vary significantly more than previously reported. Cloutis and Gaffey (1991) report that pyroxenes with Ca contents between 0 and 30 mol.% and Fe contents <65 mol.% have band centers between ∼910 and 950 nm. Similarly, spectra of synthetic pure Fe-pyroxene from Klima et al. (2007) have band centers at wavelengths lower than 950 nm. To account for such uncertainty, we include pyroxenes in our spectral library samples with a wider range of chemistries than what has been reported for Psyche.

### 2.4. Analysis of Spectral Data

Once the library was assembled, we compared laboratory spectra with telescopic observations of Psyche using a chi-square curve-matching method and by comparing measured depths and centers of any absorption features. We then convolved the library spectra to Imager filter bandpasses and explored spectral characteristics that could support future Imager operations and mapping. All data processing was performed in Python 3.6.

Our first investigation was to compare the full wavelength range of each spectrum of Psyche to the laboratory spectra. We first normalized both asteroid and sample spectra to 1.0 at 750 nm. This wavelength was chosen because it exists in all the published spectra of Psyche, is typically a local maximum in reflectance spectra of Fe-bearing silicates, and lies within a high signal-to-noise ratio region of the lab spectrophotometer used to collect data in this study. Next, we computed a chi-square goodness-of-fit statistic using the following formula:

$$\chi^2 = \frac{1}{N_w} \sum_{i=1}^{N_w} \frac{(R_i - w_i)^2}{w_i}$$

where $R_i$ and $w_i$ are the reflectance at wavelength $i$ of the meteorite and asteroid reflectance spectra, respectively, and $N_w$ is the total number of wavelengths used. The use of similar chi-square metrics to assess goodness-of-fit is well-established in asteroid spectral studies (e.g., Fornasier et al., 2010; Nedelcu et al., 2007; Ockert-Bell et al., 2010) and offers a simple way to filter a spectral library for best matches. In this context, the chi-square metric is not used to evaluate a null hypothesis using a $p$-value, but instead quantifies the difference between the spectra of Psyche and those in our library. It is essentially the same as the sum of squared residuals. Thus, a meteorite spectrum with the minimum chi-square value for a certain spectrum of Psyche represents the best fit spectrum in our library. It is important to note that this metric weights every wavelength of the two spectra equally, and thus is not sensitive to specific absorption features. We propagate the measurement uncertainty for

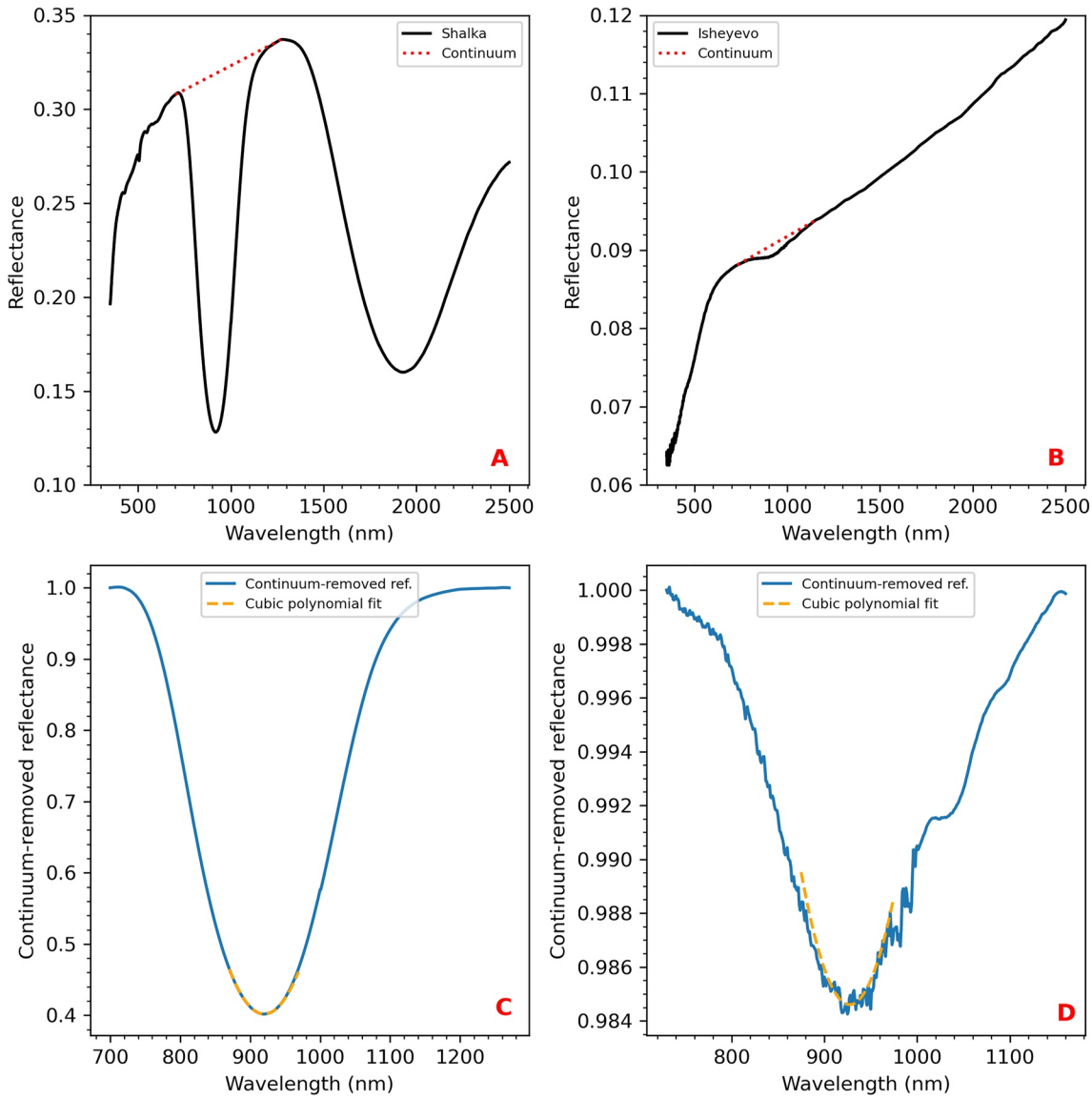


**Figure 1.** Many of the spectra in our library contain absorption features at ~1,000 nm that we compared to similar features in spectra of (16) Psyche. A spectrum of the diogenite Shalka (black line in a) exhibits strong absorption features, while spectra from the CH/CBb chondrite Isheyevo (black line in b) exhibit a weak feature comparable to Psyche. We divide the spectra by a linear continuum fit across the absorption feature (dotted red lines in panels [a and b]) and fit a third order polynomial to the minimum 40 values (dashed orange line in panels [c and d]) to determine band parameters (see text for details). For clarity, in panels (c and d) the third order polynomial is extended out to the minimum 100 values of the continuum-removed absorption feature.

the asteroid and meteorite spectra to derive an uncertainty for the chi-square metric. To match albedo values for Psyche, we filtered our library for spectra with >6% and <20% reflectance at 550 nm. The "reflectance-filtered" library used in our chi-square analysis contains 160 spectra. The chi-square goodness-of-fit metric for all spectra in the full library is available in Table S2.

Further mineralogical interpretation of an asteroid's surface requires a comparison of the center and depth of any absorption features present in the spectrum to those in laboratory spectra (Gaffey et al., 2002). We report the depth and center of any ~1,000 nm absorption features in the spectra in our library in Table S1. These parameters were calculated using the methods of Clark and Roush (1984) and Cloutis et al. (2015), which are depicted graphically in Figure 1. First, visually estimated shoulder wavelengths of any absorption feature were used to fit a straight line continuum across the absorption feature (dashed red lines in Figures 1a and 1b). The continuum was removed by dividing the sample's absolute reflectance by this continuum line (blue lines in Figures 1c and 1d). Similar to

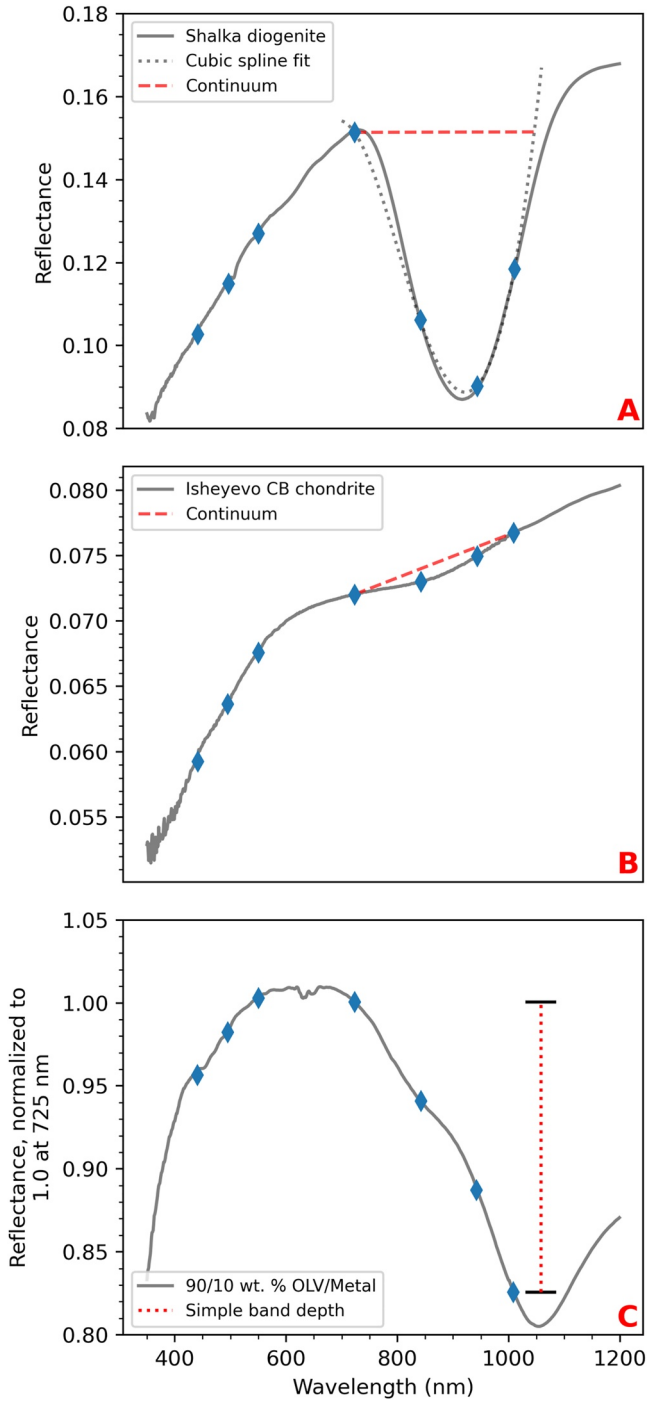


**Figure 2.** Three methods for measuring band depths and centers in spectra convolved to Imager bandpasses. High resolution laboratory spectra (gray lines) are downsampled to multispectral resolution data (blue diamonds) during the convolution process. See text for discussion.

Cloutis et al. (2015), we fit a third order polynomial to the 20 wavelengths on either side of the minimum value of the continuum-removed features (orange dashed lines in Figures 1c and 1d). The minimum value of the third order polynomial was taken to be the continuum-removed band center. Band depth was determined using Equation 32 of Clark and Roush (1984):

$$D_b = \frac{(R_c - R_b)}{R_c}$$

where $D_b$ is band depth, $R_c$ is reflectance of the continuum at the band center, and $R_b$ is the continuum-removed reflectance at the band center. This process is repeated 50 times for each absorption feature in each spectrum, using a normally distributed set of shoulder wavelengths centered on the original input shoulder wavelengths with a variance of 10 nm. We report the mean and standard deviation of the 50 calculated values for each absorption feature in each spectrum (Table S1).

### 2.5. Diagnostic Spectral Parameters

To support Imager science goals, we developed a set of parameters that can be used to identify major compositions that could potentially be found on the surface of Psyche based on potential meteorite analogs and previous telescopic observations. First, we convolve the high-resolution laboratory spectral data to the Imager's spectral throughput using the following equation:

$$I_{\lambda_1,\lambda_2} = \frac{\int_{\lambda_1}^{\lambda_2} R(\lambda) * QE(\lambda) * T(\lambda) * L_{sun}(\lambda) d\lambda}{\int_{\lambda_1}^{\lambda_2} QE(\lambda) * T(\lambda) * L_{sun}(\lambda) d\lambda}$$

where $R(\lambda)$, $QE(\lambda)$, $T(\lambda)$, and $L_{sun}(\lambda)$ are the sample reflectance, detector quantum efficiency, filter and telescope transmission, and solar radiance at wavelength $\lambda$, respectively. This process effectively downsamples the laboratory spectral data into an estimate of what the Imager would "see" if each library spectrum occurred on the surface of Psyche. To emulate probable measurement uncertainty of the Imager, we uniformly vary the reflectance at each wavelength of each input laboratory spectrum by 2%, perform the convolution 1,000 times, and then use the mean and standard deviation of the convolved values. An uncertainty of 2% is consistent with other flight instruments with similar designs and electronics to the Psyche Imager (e.g., Bell et al., 2021).

Because of variable band depths and centers of the spectra in our library, we developed three methods for measuring silicate absorption features in the Imager-convolved spectra. These are graphically depicted in Figure 2. The first method (Figure 2a) is effective for spectra with strong absorption features centered near ~948 nm (e.g., Fe-rich pyroxene). In this case, we fit a cubic spline to the convolved data from the four longest wavelength filters (725, 850, 948, and 1,041 nm). We then generated a flat "continuum" connecting the convolved point at 725 nm to a point on the cubic spline longward of 1,041 nm that had the same reflectance as the 725 nm convolved point. Then, we divided the values of the cubic spline by the flat continuum. We used the wavelength of the minimum value of the quotient as the band center and computed the band depth as the difference between the minimum continuum-removed reflectance value and 1.0.

The second method (Figure 2b) is similar to the first but is useful for spectra with strong near-infrared slopes (e.g., mixtures dominated by metal). In this case, we fit a linear continuum between the convolved values for the 725 and 1,041 nm filters. We then divided a cubic spline fit to the four near-infrared filters by this continuum. Similar to the first method, we assume the wavelength of the minimum value of the quotient as the band center and computed the band depth as the difference between the minimum continuum-removed value and 1.0.

The third method (Figure 2c) is simpler and is useful for spectra with absorption features centered at wavelengths longer than ∼1,000 nm (e.g., Fe-bearing olivine). First, the convolved data are normalized to unity at the 725 nm filter value. The band depth is then computed as the difference in the normalized convolved values for the 725 and 1,041 nm filters.

## 3. Comparison of Spectra of (16) Psyche to Laboratory Spectra

### 3.1. $\chi^2$ Goodness-Of-Fit Comparison

The five laboratory spectra with the lowest chi-square goodness-of-fit value for each spectrum of Psyche are listed in Table 3. This number of best-fitting spectra was chosen to be shown in Table 3 to be consistent with past analyses using the chi-square method (e.g., Nedelcu et al., 2007) and to show the spread of different compositions with spectra similar to Psyche (see Table S2 for all chi-square values for each sample compared to each spectrum of Psyche). Brief descriptions of the samples, their physical form (grain size/surface roughness), and the phase angle of the measurement are also listed in Table 3. Consistent with Dibb et al. (2022), we find that spectral data of Psyche are quantitatively consistent with iron meteorite powders and slabs, sulfide powders and slabs, and powder from the CH/CBb chondrite Isheyevo (Table 3).

The spectrum with the lowest chi-square value (i.e., the "best" match) is plotted over the corresponding spectrum of Psyche in Figure 3. Similar to Psyche, these materials exhibit relatively featureless, red-sloped spectra at visible to near-infrared wavelengths (Figure 3). As mentioned previously, it is important to note that the chi-square test used here weights the entire spectrum equally and is therefore not particularly sensitive to subtle absorption features. Therefore, the samples listed in Table 3 can only be interpreted as the most probable surface mineralogy for Psyche within the range of compositions sampled in our spectral library. The consistency with which certain materials have low chi-square values when compared to multiple observations of Psyche provides increased support for a comparable mineralogy between that material and the surface of the asteroid.

Consistent with previous studies, our results demonstrate similarity between reflectance spectra of Psyche and those of iron meteorite powder and/or low-Fe silicates (e.g., enstatite). For example, Cloutis et al. (1990) demonstrated that the spectrum of Psyche was intermediate in spectral properties to powder from the Odessa IAB iron meteorite and powder from the acid-insoluble fraction of the Happy Canyon enstatite chondrite. Happy Canyon is an impact melt breccia that consists of ∼85 vol.% enstatite ($Fs_{0.4}$), 5–10 vol.% $An_{26}$ plagioclase, 5 vol.% $Fs_{0.9}$ diopside, and minor Fe, Ni metal, and troilite (McCoy et al., 1995; Olsen et al., 1977).

We note, however, that enstatite chondrites are absent from the top five best spectral matches for all spectra of Psyche (Table 3). The enstatite chondrite with the lowest chi-square value for a particular spectrum of Psyche is LEW 88180. The value for this sample ranks 27th out of the 160 spectra in our reflectance-filtered library when compared to the SMASS/DeMeo et al. (2009) spectrum. The spectra of enstatite chondrites in this study have near-infrared (∼1,000–2,500 nm) spectral slopes that are lower than spectra of Psyche, which causes a high chi-square value relative to iron meteorites, sulfides, and the powder from Isheyevo. The spectral differences between enstatite chondrites and spectra of Psyche observed here are consistent with past comparisons of spectra of Psyche with meteorites (e.g., Cloutis et al., 1990; Fornasier et al., 2010; Hardersen et al., 2005). While they are a worse spectral match for Psyche than other materials in our study, the presence of an enstatite chondrite-like mineralogy on the surface of the asteroid cannot be completely ruled out. Both radar and emissivity data of Psyche are consistent with an enstatite chondrite-like surface mineralogy with areas of enhanced metal abundance (e.g., de Kleer et al., 2021; Landsman et al., 2018; Matter et al., 2013; Shepard et al., 2021). Additionally, enstatite chondrites are a likely analog composition for the only other M-type asteroid visited by spacecraft, (21) Lutetia (Vernazza et al., 2011).

Fornasier et al. (2010) found the spectrum of Psyche to be best matched by iron meteorite powder and attributed a subtle absorption feature at ∼900 nm to low-Fe, low-Ca orthopyroxene. A connection between Psyche and the

**Table 3**
*Best Chi-Square Matches for (16) Psyche for Spectra in Our Library After Filtering for Reflectance >6% and <20% at 550 nm*

| (16) Psyche spectrum reference | ID/Spectrum name | Sample name (type) | Grain size (μm)/ surface roughness | Phase angle (*i*/*e*) | $\chi 2$ ($\times 10^6$) |
|---|---|---|---|---|---|
| SMASS/DeMeo et al. (2009) | 30_06 | Isheyevo powder (CH/CBb) | >75 | 23/8 | 290 ± 2 |
| | mar0207.060 | MET01A (iron met.) | <45 | 60/−30 | 390 ± 29 |
| | mar0207.036 | MET01A (iron met.) | <45 | 60/60 | 400 ± 31 |
| | 30_02 | Isheyevo powder (CH/CBb) | <1,000 | 38/8 | 420 ± 3 |
| | MPMIX 1011 | MET101A (iron met.) | <45 | 35/0 | 450 ± 31 |
| Hardersen et al. (2005) | mar0707a.004 | MET01A (iron met.) | <45 | 30/60 | 180 ± 23 |
| | 30_07 | Isheyevo powder | <75 | 53/8 | 190 ± 7 |
| | feb1607.006 | MET02A (iron met.) | <45 | 30/0 | 390 ± 37 |
| | feb1607.009 | MET03A (iron met.) | <45 | 30/0 | 400 ± 34 |
| | mar0107.004 | MET01A (iron met.) | <45 | 0/30 | 400 ± 37 |
| Fornasier et al. (2010) | 25_07 | Gibeon powder (iron met.) | >75 | 23/8 | 840 ± 23 |
| | 25_05 | Gibeon powder (iron met.) | >75 | 38/8 | 1,250 ± 29 |
| | 39_05 | Sikhote-Alin powder (iron met.) | >75 | 23/8 | 1,400 ± 27 |
| | 39_07 | Sikhote-Alin powder (iron met.) | >75 | 53/8 | 1,430 ± 29 |
| | feb1607.007 | MET02B (iron met.) | 45–90 | 30/0 | 1,790 ± 77 |
| Sanchez et al. (2017)—2015 December 08 10:30 | 35_02 | Auburn FeS powder (sulfide) | <1,000 | 38/8 | 140 ± 4 |
| | 35_03 | Auburn FeS powder (sulfide) | <75 | 38/8 | 200 ± 6 |
| | mar0207.012 | MET01A (iron met.) | <45 | 30/30 | 310 ± 29 |
| | 41_02 | MTMIX2 (metal-sulfide mix) | <75 | 38/8 | 340 ± 6 |
| | 35_04 | Auburn FeS powder (sulfide) | >75 | 38/8 | 340 ± 7 |
| Sanchez et al. (2017)—2015 December 08 11:43 | 30_07 | Isheyevo powder (CH/CBb) | <75 | 53/8 | 410 ± 33 |
| | mar0107.004 | MET01A (iron met.) | <45 | 0/30 | 410 ± 8 |
| | mar0707a.004 | MET01A (iron met.) | <45 | 30/60 | 430 ± 36 |
| | 35_02 | Auburn FeS powder (sulfide) | <1,000 | 38/8 | 510 ± 10 |
| | 35_03 | Auburn FeS powder (sulfide) | <75 | 38/8 | 600 ± 11 |
| Sanchez et al. (2017)—2015 December 08 12:47 | mar0707a.004 | MET01A (iron met.) | <45 | 30/60 | 340 ± 30 |
| | feb1607.009 | MET03A (iron met.) | <45 | 30/0 | 390 ± 35 |
| | feb1607.006 | MET02A (iron met.) | <45 | 30/0 | 400 ± 35 |
| | 30_07 | Isheyevo powder (CH/CBb) | <75 | 53/8 | 450 ± 6 |
| | mar0107.004 | MET01A (iron met.) | <45 | 0/30 | 650 ± 42 |
| Sanchez et al. (2017)—2015 December 08 14:01 | feb1607.010 | MET03B (iron met.) | 45–90 | 30/0 | 160 ± 21 |
| | 41_01 | MTMIX1 (metal-sulfide mix) | <75 | 38/8 | 180 ± 3 |
| | feb1607.008 | MET02C (iron met.) | 90–250 | 30/0 | 240 ± 25 |
| | feb1607.004 | MET01B (iron met.) | 45–90 | 30/0 | 240 ± 26 |
| | 25_08 | Gibeon powder (iron met.) | <75 | 53/8 | 280 ± 3 |
| Sanchez et al. (2017)—2016 February 10 05:10 | 36_01 | Del Norte County FeS slab (sulfide) | 1,200 grit | 38/8 | 130 ± 1 |
| | feb1607.010 | MET03B (iron met.) | 45–90 | 30/0 | 340 ± 30 |
| | 38_07 | Minas Gerais Pyrrhotite (sulfide) powder | >75 | 53/8 | 340 ± 2 |
| | 41_01 | MTMIX1 (metal-sulfide mix) | <75 | 38/8 | 420 ± 2 |
| | 25_04 | Gibeon powder (iron met.) | <75 | 38/8 | 430 ± 2 |
| Sanchez et al. (2017)—2016 February 10 05:30 | C1AG03 | AG-BXR-003 Pentlandite powder (sulfide) | 212–600 | 30/0 | 180 ± 72 |
| | feb1607.005 | MET01C (iron met.) | 90–250 | 30/0 | 420 ± 33 |

**Table 3**
*Continued*

| (16) Psyche spectrum reference | ID/Spectrum name | Sample name (type) | Grain size (μm)/ surface roughness | Phase angle (*i*/*e*) | $\chi 2$ ($\times 10^6$) |
|---|---|---|---|---|---|
| | 32_01 | Nickel sulfide, hand sample (sulfide) | hand sample | 30/0 | 530 ± 2 |
| | feb1607.009 | MET03A (iron met.) | <45 | 30/0 | 710 ± 42 |
| | feb1607.006 | MET02A (iron met.) | <45 | 30/0 | 730 ± 43 |
| Sanchez et al. (2017)—2016 February 10 06:34 | C1AG03 | AG-BXR-003 Pentlandite powder (sulfide) | 212–600 | 30/0 | 140 ± 55 |
| | feb1607.005 | MET01C (iron met.) | 90–250 | 30/0 | 150 ± 21 |
| | feb1607.009 | MET03A (iron met.) | <45 | 30/0 | 270 ± 26 |
| | feb1607.006 | MET02A (iron met.) | <45 | 30/0 | 290 ± 27 |
| | 39_02 | Sikhote-Alin powder (iron met.) | <75 | 38/8 | 700 ± 2 |
| Sanchez et al. (2017)—2016 February 10 08:05 | 32_01 | Nickel sulfide, hand sample (sulfide) | hand sample | 30/0 | 510 ± 2 |
| | C1AG03 | AG-BXR-003 Pentlandite powder (sulfide) | 212–600 | 30/0 | 740 ± 129 |
| | feb1607.005 | MET01C (iron met.) | 90–250 | 30/0 | 1,060 ± 55 |
| | feb1607.009 | MET03A (iron met.) | <45 | 30/0 | 1,060 ± 52 |
| | feb1607.006 | MET02A (iron met.) | <45 | 30/0 | 1,080 ± 53 |

metal-rich CB/CH chondrites (e.g., Isheyevo) was discouraged by Hardersen et al. (2011) because the long wavelength band center measured for Psyche (>940 nm) was thought to be inconsistent with the low-Fe silicates seen in CB/CH chondrites. However, our results, in combination with studies showing the variation in band center with Fe in pyroxenes (e.g., Cloutis & Gaffey, 1991; Klima et al., 2007), suggests that a link could still exist. Furthermore, Shepard et al. (2021) and de Kleer et al. (2021) measured radar and millimeter emissivity and polarization that is consistent with a CB chondrite-like composition with a near-surface porosity of 75%. Isheyevo is made up of two distinct lithologies (metal-rich/CBb-like and metal-poor/CH-like) and exhibits laminar features interpreted as evidence of gentle reaccretion of material in the impact plume of a glancing collision between planetesimals (Garvie et al., 2017; Ivanova et al., 2008; Krot et al., 2007; Morris et al., 2015). Isheyevo is ∼60 vol.% metal and its ferromagnesian chondrules are typically Fe-poor (Ivanova et al., 2008). If Psyche is indeed a mixture of core and mantle materials, identification of a metal-silicate mixture like Isheyevo using both Imager and GRNS data could offer strong constraints on any impact(s) that led to Psyche's current state.

We note that it is unlikely that other types of carbonaceous chondritic material dominate the surface composition of Psyche. Generally, spectra from carbonaceous chondrites are too dark, too blue-sloped (decreasing reflectance with increasing wavelength), and/or exhibit relatively strong absorption features not found in spectra of Psyche (Cloutis, Hiroi, et al., 2011; Cloutis, Hudon, et al., 2011; Cloutis et al., 2012a, 2012b, 2012c, 2012d, 2012e, 2012f). However, the variations in Psyche's albedo, spectral reflectance, radar reflectivity, and emissivity suggest that residual material from infalling carbonaceous chondritic impactors could be present on the surface. This would be consistent with observations of carbonaceous material on the surface of (4) Vesta (e.g., Reddy et al., 2012), dynamical studies of the possibility of infall of hydrated material (e.g., Avdellidou et al., 2018), and the results of Cantillo et al. (2021) demonstrating that a spectrum of Psyche is consistent with a mixture of metal, low-Fe pyroxene, and powder from the Murchison CM2 chondrite.

Other meteorite types that have been associated with Psyche include mesosiderites (e.g., Sanchez et al., 2017; Viikinkoski et al., 2018) and ureilites (e.g., Goodrich et al., 2018; Hardersen et al., 2005). Mesosiderites are mixtures of metal, basaltic, gabbroic, and/or pyroxenitic silicates, and sulfides like troilite. These meteorites are typically >40 wt.% silicates, the majority of which is pyroxene with >20 mol.% Fe (Mittlefehldt et al., 1998). Spectra of mesosiderites exhibit 1,000 nm absorption features with band depths that exceed those measured in spectra of Psyche as well as ∼1,900 nm features absent in spectra of Psyche (this study and Burbine, Greenwood, et al., 2007). Thus, it is unlikely that Psyche's surface is dominated by a mesosiderite-like lithology. Ureilites, which are carbon-bearing ultramafic meteorites dominated by olivine and pyroxene, have been invoked as a possible precursor material for M-type asteroids like Psyche that underwent a high-temperature (>850°C) smelting reaction (Hardersen et al., 2005; Mittlefehldt et al., 1998). The olivine and pyroxene in these meteorites typically

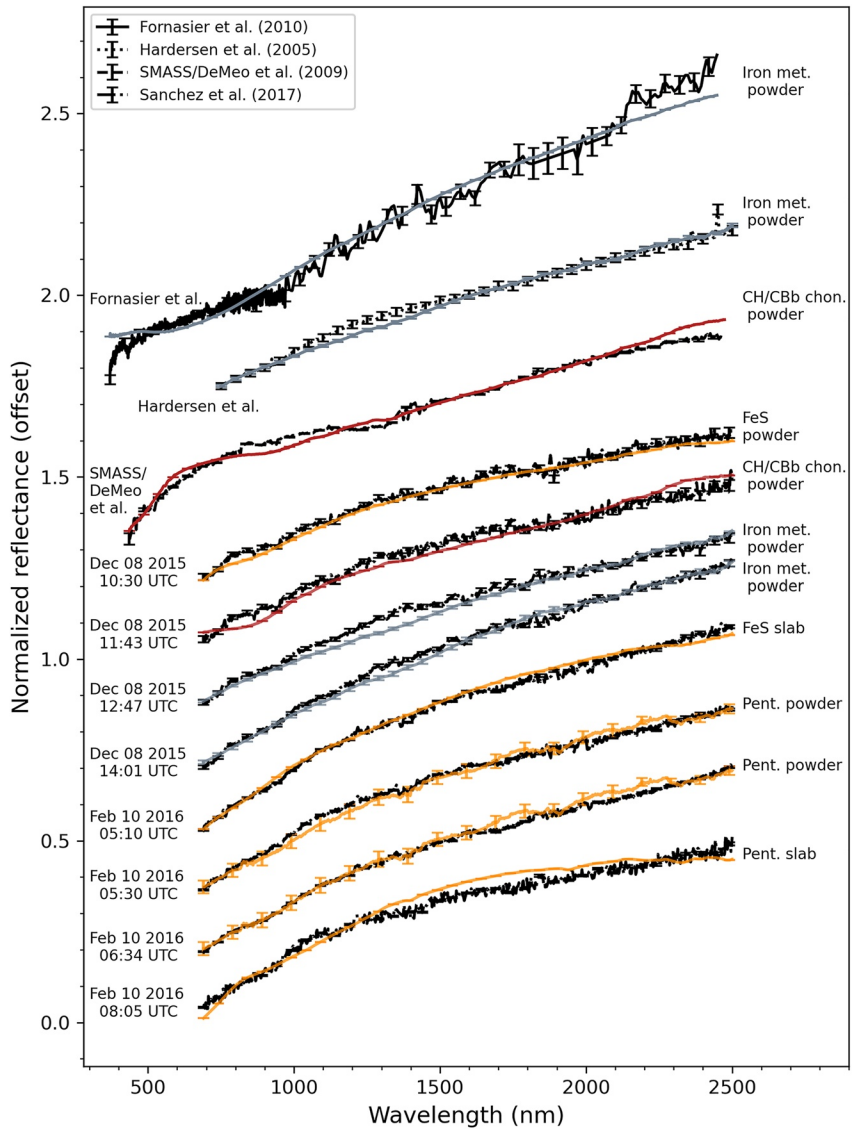


**Figure 3.** Reflectance spectra of (16) Psyche (black) plotted with their best fit spectrum in our library (red—CH/CBb chondrite, gray—iron meteorites, yellow—sulfide). "Best fit" was determined by which spectrum had the minimum chi-square value. Spectral data of Psyche are from Fornasier et al. (2010) (solid black), Hardersen et al. (2005) (dotted black), the Small Main-Belt Asteroid Spectral Survey (Bus & Binzel, 2002; DeMeo et al., 2009, dashed black), and Sanchez et al. (2017) (dash-dot black). The multiple observations from Sanchez et al. (2017) are labeled by observation time (lower 8 spectra).

contain >10–15 mol.% Fe (Mittlefehldt et al., 1998). The smelting reaction would have reduced this Fe-bearing olivine (fayalite) in the precursor material to Fe-free pyroxene, metal, carbon dioxide, and silica, proceeding at a rate dependent on the limiting reactant (either carbon or fayalite; Hardersen et al., 2005). However, the presence of some Fe-bearing pyroxene on Psyche (inferred from observed band centers) implies incomplete reduction of the fayalite component, which would theoretically remain on the surface. Spectra of ureilites and low-Fe fayalite have band centers >1,000 nm, and thus its presence on the surface of Psyche is not supported by current observations of the asteroid. Thus, it is unlikely that ureilite-like material currently exists on Psyche's surface (Hardersen et al., 2005).

The interpretation that the surface of Psyche could be enriched in (and possibly dominated by) sulfide minerals is relatively new. Fornasier et al. (2010) attributed some reflectance features at ~490 nm in the spectrum of Psyche to sulfide minerals like troilite and/or oldhamite. The densities of troilite (~4.8 g/cm$^3$) and pentlandite (~4.9 g/cm$^3$)

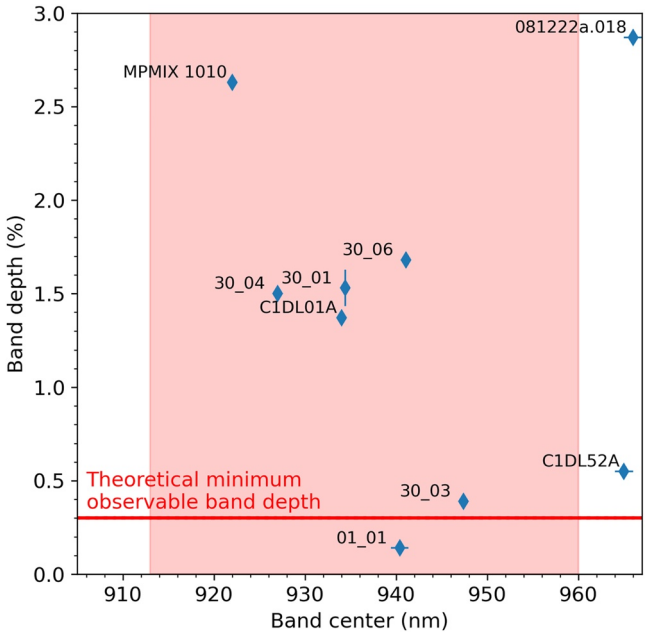


**Figure 4.** The range of reported ~1,000 nm band centers and depths of spectra of (16) Psyche (pink region) are consistent with band parameters from samples containing metal and/or low-Fe, low-Ca pyroxene (e.g., enstatite). Samples with the "30_…" prefix are samples of the CH/CBb chondrite Isheyevo. Sample 01_01 is a hand sample of the aubrite Mayo Belwa. MPMIX1010 is a powder mixture of 90 wt.% iron meteorite metal and 10 wt.% $En_{50.8}$ $Fs_{45.6}$ orthopyroxene (Cloutis et al., 2009). Samples C1DL01A and C1DL52A are synthetic pyroxenes with $En_{100}$ and $En_{90}Wo_{10}$ compositions, respectively (Klima et al., 2007). Sample 081222a.018 is powder from the EH4 chondrite MET 00783. The red line represents the theoretical minimum observable band depth measurable by the Imager.

are within the range of values reported for Psyche (Elkins-Tanton et al., 2020; Siltala & Granvik, 2021). Furthermore, de Kleer et al. (2021) measured thermal inertia and millimeter emissivity values of Psyche that are consistent with sulfides dominating the "metallic" portion of the asteroid, with a surface porosity of 40%. Sulfide minerals are common in both chondritic and achondritic meteorites (e.g., Mittlefehldt et al., 1998; Scott & Krot, 2003) and can form both directly from the solar nebula (Lauretta et al., 1997) and through both high and low-temperature processes expected during planetary formation (Schrader et al., 2016 and references therein). While few meteorites with high abundances (tens of vol.%) of sulfide minerals exist in terrestrial collections, models of trace element behavior in iron meteorites suggest that sulfur may have been present in high enough abundance during early planetesimal core formation to form an immiscible sulfide liquid (Bercovici, 2020; Chabot, 2004; Goldstein et al., 2009; Ulff-Møller, 1998). If Psyche is indeed composed of remnant core materials, a significant amount of sulfide material could remain detectable on the surface (e.g., Dibb et al., 2022). However, constraining the exact nature of any sulfide components on the surface of Psyche from reflectance spectroscopy remains challenging due to spectral differences between natural and synthetic sulfides and the limited number of spectra of natural oldhamite (e.g., Burbine et al., 2002; Helbert et al., 2013; Varatharajan et al., 2019). Further reanalysis of Psyche's properties in the context of sulfide minerals could help to constrain this hypothesis.

Finally, while Binzel et al. (1995) initially observed no rotational spectral variations for Psyche at visible wavelengths <900 nm, a more recent study in the near-infrared by Sanchez et al. (2017) reported rotational variations that were detectable in the band center of the ~1,000 nm feature. This variation in band center was interpreted by the authors as evidence for variation in the abundance and chemistry of a purported pyroxene component. We note that the two studies of rotational variation are not mutually exclusive: Binzel et al. (1995) observed Psyche at a nearly equatorial latitude while Sanchez et al. (2017) were observing at ~−46° and ~−52° latitude. Similar to Sanchez et al. (2017), our chi-square results suggest that there could be significant compositional variation on the surface of the asteroid. This is further supported by variations in radar reflectivity and millimeter emissivity (e.g., Cambioni et al., 2022; de Kleer et al., 2021; Shepard et al., 2021) that are correlated with changes in optical albedo, consistent with potential variation in the metal-silicate ratio across the surface of the asteroid.

### 3.2. Comparison of Band Parameters

Surface mineralogy can also be constrained by comparing the depths and centers of absorption features at ~1,000 nm in the spectra in our library to telescopic spectra of Psyche (Figure 4). Similar to previous studies, our band parameter measurements suggest that the surface of Psyche is consistent with a metal-rich composition mixed with a silicate component. An example of this is the 90/10 wt.% mixture of powder from the Odessa iron meteorite and $Fs_{45.6}$ orthopyroxene from Cloutis et al. (2009), labeled MPMIX1010 in Figure 4. We note that the pyroxene in this mixture is more Fe-rich ($En_{50.8}$ $Fs_{45.6}$) than what is typically inferred from telescopic spectra of Psyche.

Of the three types of materials with minimized chi-square values (iron meteorites, sulfides, and powder from Isheyevo), only spectra from Isheyevo exhibit an absorption feature at ~1,000 nm consistent with absorption features seen in spectra of Psyche. In Figure 4, points labeled with a "30_" prefix are samples from Isheyevo. The scatter in points from this sample is consistent with previous measurements of variation in band depth and center as grain size and phase angle vary. Samples 30_03 and 30_04 are from <75 micron and >75 micron fractions of powder from Isheyevo, respectively. Both spectra were measured at a phase angle of (*i*/*e*) 38°/8°. The finer fraction (sample 30_03) exhibits a shallower absorption feature (consistent with trends for finer grained pyroxene)

and a longer wavelength band center (consistent with a shift caused by blue-sloped spectra of finer grained metal; Cloutis et al., 1990; Cloutis et al., 2010). Additionally, it is possible that sample 30_03 has a higher proportion of iron-bearing silicates (e.g., pyroxene and olivine) than the coarser fraction due to the ease with which silicates are comminuted compared to metal. The higher relative abundance of olivine compared to metal could shift the band center to longer wavelengths (e.g., Cloutis et al., 1990). Furthermore, spectra from the powders of Isheyevo at the same grain size but different phase angle (i.e., 30_04 at *i*/*e* 38°/8° and 30_06 at *i*/*e* 23°/8°) are consistent with published trends for metal-rich compositions. For example, Cloutis et al. (2010) measured decreasing spectral slope with decreasing phase angle for iron meteorite powders. With a lower (or even negative) spectral slope, the band center of metal-silicate mixtures could shift to longer wavelengths relative to a spectrum of the metal-silicate mixture measured at a larger phase angle.

Absorption band parameters from a hand sample of the aubrite Mayo Belwa (sample 01_01 in Figure 4) are also consistent with those of Psyche. Like other aubrites, this meteorite is composed mostly of almost Fe-free enstatite (97.5 vol.% $En_{99}$; Watters & Prinz, 1979). Another enstatite-rich sample, the enstatite chondrite MET 00783 (sample 081222a.018), exhibits a band center slightly longward of the upper range of reported band parameters for Psyche. MET 00783 is mostly enstatite (67 wt.%) with troilite (12 wt.%), albite (6 wt.%), kamacite (6 wt.%), and gypsum (5 wt.%) (Izawa et al., 2010). The presence of albite and gypsum (terrestrial weathering products), which exhibit broad absorption features centered at ∼1,200 and 1,400 nm, respectively, may be the cause of the longer wavelength center of MET 00783. Finally, absorption features of $En_{100}$ and $En_{90}Wo_{10}$ synthetic pyroxenes from Klima et al. (2007) (samples C1DL01A and C1DL52A, respectively) are also consistent with reported band depths and band centers for Psyche.

Also shown in Figure 4 is a theoretical minimum observable band depth that the Imager can measure (∼0.3%). This limit is based on radiometric modeling of the Imager's performance during nominal Orbit B operations using equations from Tables 9–15 in Larson and Wertz (1999). We use this radiometric model to estimate the signal-to-noise ratio (SNR) for pixels in images taken through each filter. During Orbit B operations, we estimate the SNR in the two longest wavelength filters (centered at 948 and 1,041 nm) to be ∼118 and ∼98, respectively, assuming pixel summing ($2 \times 2$ and $3 \times 3$, respectively) and the longest possible exposure times before the spacecraft's velocity causes smearing of a half-pixel (167.4 and 251.1 ms, respectively). These SNR estimates translate to relative errors of 0.85% and 1.02%. Assuming Psyche's albedo at 1,000 nm is ∼0.14, these relative errors translate to absolute reflectance uncertainties of ∼0.12% and 0.14%. The sum of these two absolute reflectance uncertainties represents the theoretical minimum observable band depth (∼0.3%). This limit suggests that absorption features from very low-Fe natural pyroxenes, like those in spectra of Mayo Belwa, could be undetectable by the Imager. However, very low-Fe enstatite-rich compositions (e.g., aubrites) are typically much brighter than the measured visible wavelength reflectance of Psyche, and thus current observations suggest that these compositions are not likely to occur on the asteroid's surface.

## 4. Preliminary Strategies for Using Imager Data to Assess Surface Composition

Three of the five major science objectives of the Psyche mission that require data from the Imager filters are: (a) to determine if Psyche is a remnant planetary core; (b) to determine if small bodies incorporate the same light elements as are expected in the Earth's core; and (c) to determine the redox conditions under which Psyche was formed (Elkins-Tanton et al., 2016, 2020). To address these objectives, the Imager must assess the homogeneity of metal-silicate mixing, identify any diagnostic sulfur-bearing phases present, and discriminate between silicate or sulfide compositions that could help to constrain redox conditions (Bell et al., 2016; Elkins-Tanton et al., 2020, 2022). Using the laboratory spectra in our library, we have developed a set of parameters using spectra convolved to the Imager's spectral throughput that could allow rapid processing of future Imager multispectral data to derive compositional information about the surface of Psyche at the resolution of single images, and thus to help address the mission's relevant science objectives.

While the generally featureless, red-sloped spectra from most disk-integrated telescopic measurements of the asteroid (Table 2) are typically interpreted as evidence of a surface dominated by metal but potentially with some low-Ca, low-Fe silicates, they do not rule out the possibility of small (unresolved) areas on the surface enriched in silicate minerals with higher Ca or Fe contents (e.g., MPMIX1010 in Figure 4). This possibility is consistent with the rotational spectral variation reported by Sanchez et al. (2017), who measured areas of differing silicate abundance and chemistry heterogeneously distributed on the surface of Psyche. Thus, it is prudent to explore how

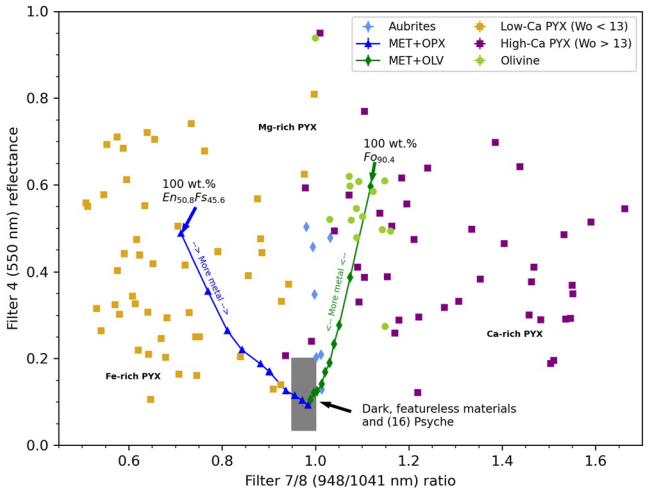


**Figure 5.** Low-Ca pyroxene (Wo < 13, yellow squares) can be discriminated from other silicates that could be present on the surface of Psyche, like high-Ca pyroxene (purple squares) or olivine (green circles) using the ratio between Imager Filters 7/8 (948/1,041 nm). Furthermore, these iron-bearing silicates can be discriminated from lower reflectance, featureless materials using both the Filter 7/8 ratio and the Filter 4 (550 nm) reflectance. The range of values for Psyche, iron meteorites, sulfides, and metal-rich chondrites are represented by a gray rectangle. Mixtures of pyroxene and metal (MET + OPX, dark blue triangle and solid line) and mixtures of olivine and metal (MET + OLV, dark green diamonds and solid line) at 10 wt.% intervals indicate that mixtures with increasing metal content exhibit lower 550 nm reflectance and become "featureless" (948/1,041 nm ratio of ~1.0). Uncertainty is typically smaller than the size of the points.

the Imager could discriminate various compositions with higher abundances of silicates and/or variable silicate chemistries.

For example, the nature of iron-bearing silicates relevant to Psyche (e.g., pyroxene and olivine) can potentially be constrained via the ratio of the 948/1,041 nm filter reflectances plotted versus the 550 nm filter reflectance (Figure 5). Low-Ca, Fe-bearing pyroxenes (yellow squares in Figure 5) typically exhibit an absorption feature between ~910 and ~960 nm due to $Fe^{2+}$ in the M2 crystallographic site (Adams, 1974; Cloutis & Gaffey, 1991; Klima et al., 2007). This is expressed in Imager data as a ratio in the convolved data from the 948/1,041 nm filters less than 1. Conversely, spectra of high-Ca pyroxene (purple squares in Figure 5) and olivine (green circles in Figure 5) exhibit absorption features at wavelengths longer than ~1,000 nm, and thus the 948/1,041 nm ratio is typically greater than 1. High-Mg silicates (e.g., some of the olivines and pyroxenes shown in Figure 5 as well as the aubrites) have much shallower or no absorption features, and thus exhibit 948/1,041 nm filter ratios close to 1. Most pure silicates in our library exhibit higher reflectance than the range of values reported for Psyche, represented in Figure 5 by a gray box. The more metal-rich compositions (e.g., iron meteorites, enstatite and CB chondrites) and sulfides also plot within the gray box in Figure 5. Finally, mixtures of iron meteorite metal and $Fo_{90.4}$ olivine (green diamonds in Figure 5) and iron meteorite metal and $En_{50.8}$ $Fs_{45.6}$ orthopyroxene (blue triangles in Figure 5) from Cloutis et al. (2009) are also shown in Figure 5. Both of these sets of mixtures exhibit lower 550 nm filter reflectance and become featureless (i.e., migrate toward a 948/1,041 nm filter ratio of 1) with increasing metal content.

Second, some relationships among absorption feature parameters that have been well-established from previous high spectral resolution laboratory studies can also be recovered from spectra in our library convolved to the Imager's spectral throughput. For example, Figure 6 shows the band centers reconstructed from Imager-convolved spectra of natural and synthetic pyroxenes plotted against the band center derived from the high-resolution laboratory spectra. The pyroxenes in Figure 6 are those that have chemistries within the range measured by Sanchez et al. (2017). The residual mean squared error (RMSE) from this comparison is 6.6 nm. Using the equations developed by Burbine, Buchanan, and Binzel (2007) for relating the ~1,000 nm band center in spectra of HED meteorites to their chemistry, our RMSE translates to an uncertainty in the inferred pyroxene chemistry of ±8.5 mol.% En, ±6.8 mol.% Fs, and ±2.7 mol.% Wo. Accurate measurement of absorption band centers may be used to constrain the Fe content in silicates as well as the pyroxene/olivine ratio on the surface, and thus provide insight into the redox state of the asteroid (e.g., Hardersen et al., 2005; McSween, 1992).

Furthermore, the abundance of pyroxene in metal-pyroxene mixtures can be accurately measured from Imager-convolved spectra by comparing band depths of spectra convolved to the Imager's throughput to band depths from high-resolution laboratory spectra (Figure 7a) (RMSE = 2.14%). Band depths of spectra from metal-olivine mixtures (Figure 7b) can be measured from Imager-convolved data using Method 3 in Figure 2. For mixtures with high abundance of metal, band depths become increasingly shallow and the overall spectra become more red-sloped. Band depths from mixtures with >40 wt.% olivine measured from Imager-convolved spectra can be accurately recreated, and a cubic polynomial can be used to infer band depth for mixtures with <40 wt.% olivine (Figure 7b). The RMS error for this cubic polynomial fit to the metal-olivine band depths is 3.71%.

In Figure 8 we offer a preliminary strategy for discriminating the low reflectance, "featureless" compositions that could be present on the surface of the asteroid as suggested by remote sensing and our chi-square analysis. These compositions include iron meteorites, sulfides, and CB and enstatite chondrites. Figure 8 shows the Filter 4/8 (550/1,041 nm) ratio versus the Filter 3/4 (495/550 nm) ratio for spectra from these compositions in our library that had ~1,000 nm band depths of <3.0% measured from Imager-convolved spectra. This limit is approximately the highest reported band depth in spectra of Psyche (Table 2). The Filter 3/4 (495/550 nm) ratio effectively separates the iron meteorites and sulfides due to the typically higher visible wavelength slopes of sulfides. Britt

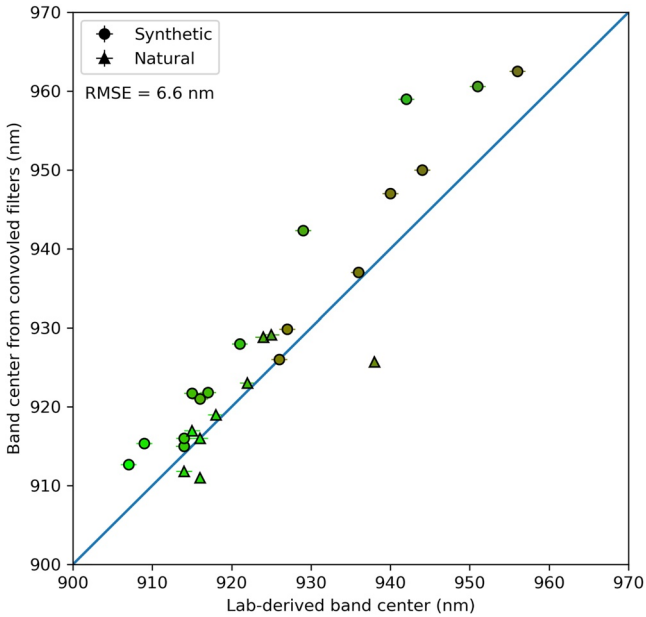


**Figure 6.** Band centers from synthetic (circles) and natural pyroxenes (triangles) can be measured in spectra convolved to the Imager's bandpasses (RMS error = 6.6 nm). The samples shown here have compositions covering the range of inferred pyroxene chemistries on the surface of Psyche by Sanchez et al. (2017). This includes all pyroxenes in our library with Fs ≤ 51.5 mol.% and Wo ≤ 12.9 mol.%. Points are colored according to their chemistry using an R/G/B = Fe/Mg/Ca scheme. Because the pyroxene on Psyche reported in Sanchez et al. (2017) is mostly Mg-rich, most points are green/brown. The blue line of slope equal to 1 indicates perfect recreation of the band center in the Imager-convolved spectra.

and Pieters (1988) and Cloutis et al. (2010) demonstrated that spectra of iron meteorites at various grain sizes and compositions are relatively invariant at these wavelengths, and this is reflected by the clustering of iron meteorites in Figure 8.

Conversely, sulfides exhibit a larger range of Filter 4/8 (550/1,041 nm) and Filter 3/4 (495/550 nm) ratios (Figure 8), likely due to the textural and mineralogical variation in the sulfide samples in our library (Table S1). Unlike the other sulfides, a cluster of points from spectra of a sulfide sample from Del Norte County, California exhibits Filter 4/8 (550/1,041 nm) ratios >0.8. This sample is dominated by troilite and pyrrhotite, but also contains a significant amount (<~20 vol.%) of cubanite ($CuFe_2S_3$). This mineral exhibits a shallower near-infrared spectral slope consistent with other Cu-bearing Fe-sulfides, which is likely the cause of Filter 4/8 (550/1,041 nm) ratios closer to 1.0 (Pirard et al., 2008; Wood & Strens, 1979). While cubanite has been found in CI chondrites (Berger et al., 2011), material returned from comet 81P/Wild 2 (Brownlee, 2014), and in exogenous regolith grains in Itokawa (Burgess & Stroud, 2021), cubanite is only found in metal-rich meteorites as a terrestrial alteration product (Rubin, 1997; Rubin & Ma, 2017). The presence of cubanite in extraterrestrial materials constrains the maximum temperature experienced to <~250°C (Berger et al., 2015), and thus identification of cubanite on the surface of Psyche could significantly constrain the asteroid's formation history.

Finally, "featureless" spectra of the CB and enstatite chondrites in our library exhibit Filter 3/4 (495/550 nm) and Filter 4/8 (550/1,041 nm) ratios distinct from the iron meteorites. We include enstatite chondrites in this plot because their spectra at Imager-relevant wavelengths (~400–1,100 nm) are comparable to spectra of Psyche (despite their near-infrared spectra deviating from those of Psyche) and because they have been previously invoked as possible Psyche analogs. Both the enstatite chondrites and CB chondrites are characterized by a high abundance of low-Fe, low-Ca pyroxene and/or olivine in chondrules (20–80 vol.%) mixed with metal, and sulfides. Some of the enstatite chondrites also contain several wt.% feldspar and terrestrial alteration products (e.g., gypsum). The enstatite chondrite MAC 02747 exhibits a Filter 3/4 (495/550 nm) ratio much lower than the other enstatite chondrites in our study. This sample has the lowest metal content of the enstatite chondrites in Figure 8 (Izawa et al., 2010), and thus may have an enhanced metal-oxygen charge transfer absorption relative to the other enstatite chondrites. This enhancement may result in a stronger visible slope and thus lower Filter 3/4 (495/550 nm) ratio.

## 5. Conclusions

The Psyche mission will explore the solar system's largest M-type asteroid, (16) Psyche. We have assembled a library of laboratory spectra that are consistent with current uncertainties in Psyche's surface composition based on spectral properties, density, radar reflectivity, and emissivity. We have performed a chi-square analysis that has shown that available telescopic spectra of Psyche, while consistent with iron meteorites, are also consistent with sulfide minerals (e.g., troilite and pentlandite) and powder from the CH/CBb chondrite Isheyevo. Second, we have compared band centers of ~1,000 nm absorption features found in spectra of Psyche to similar features in the spectra in our library. Results from this investigation are consistent with previous interpretations of the asteroid's surface being metal-rich with a low-Fe, low-Ca pyroxene component, but are also consistent with a metal-rich composition mixed with a small abundance of Fe-rich pyroxene (e.g., 90 wt.% iron meteorite metal and 10 wt.% $En_{50.8}$ $Fs_{45.6}$ orthopyroxene). Our investigation provides new insight into the surface composition of the asteroid and is consistent with recent studies that suggest the surface composition of Psyche may not be as metallic as once thought.

To address the Psyche mission's science objectives and to resolve these various compositional possibilities, the Psyche spacecraft's Multispectral Imager will map the surface from orbit at visible to near-infrared wavelengths

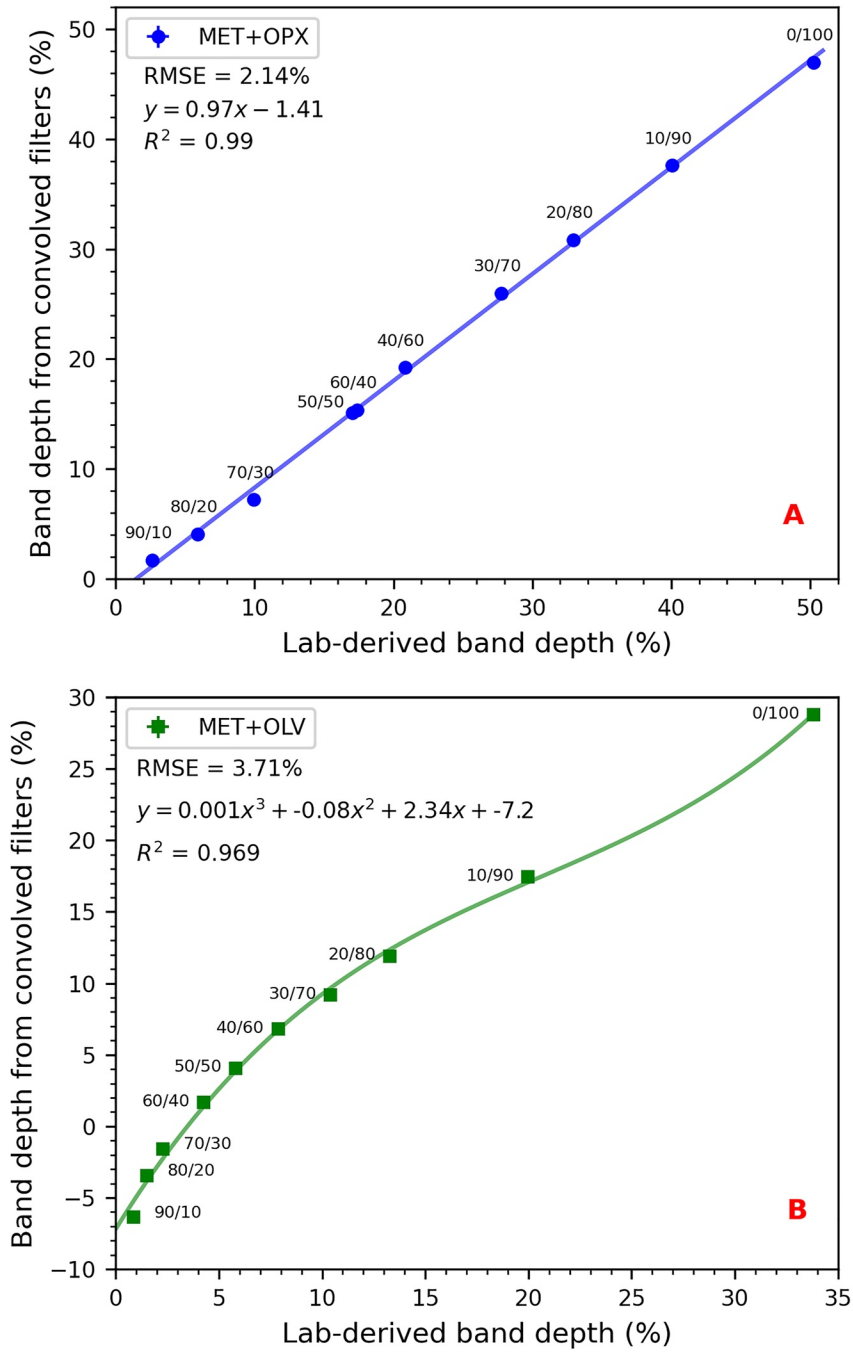


**Figure 7.** Band depths from high-resolution laboratory spectra and Imager-convolved spectra of metal-orthopyroxene mixtures (a) and metal-olivine mixtures (b) from Cloutis et al. (2009). The ratio of the components (in wt.% intervals of metal/silicates) is shown next to each point.

and at high spatial resolution. We have demonstrated that spectra of silicates and metal-silicate mixtures convolved to the Psyche Imager's filters can be discriminated based on their Filter 4 (550 nm) reflectance and Filter 7/8 (948/1,041 nm) ratio. Band centers derived from Imager-convolved data are predicted to be accurate to within <10 nm, while band depths derived from spectra of metal-silicate mixtures are predicted to be accurate to within about 5%. Finally, the low reflectance, "featureless" materials in our spectral library that are consistent with telescopic spectra of Psyche can be discriminated using the Imager Filter 3/4 (495/550 nm) and Filter 4/8 (550/1,041 nm) ratios. Multispectral images acquired by the Imager, in combination with data from the

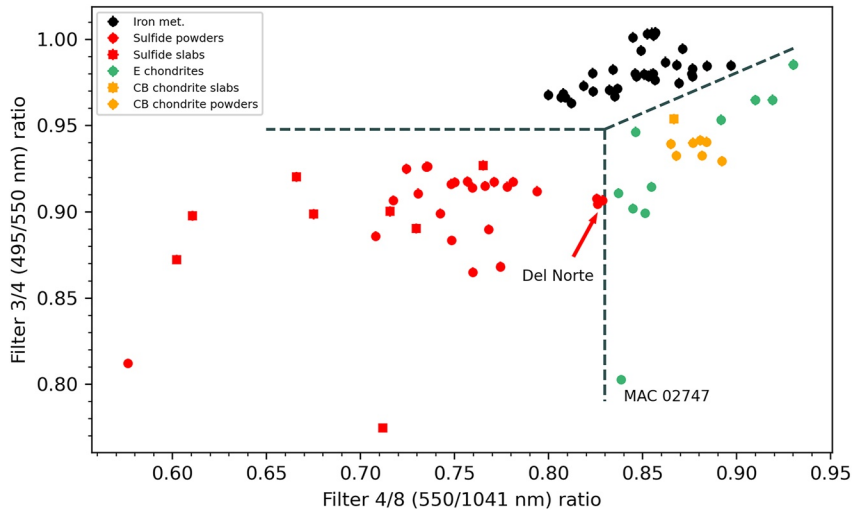


**Figure 8.** Compositions with "featureless" spectra that are consistent with telescopic spectra of (16) Psyche can be discriminated based on ratios between Filters 4/8 (550/1,041 nm) and Filters 3/4 (495/550). Spectra of powder from terrestrial sulfides from Del Norte County, California and an outlier enstatite chondrite, MAC 02747, are labeled. The Del Norte sulfide is dominated by troilite and pyrrhotite with minor cubanite ($CuFe_2S_3$). MAC 02747 has the lowest metal content of the enstatite chondrites in this study. See text for discussion.

spacecraft's GRNS and magnetometer investigations, will allow hypotheses of the asteroid's formation history to be tested and help to constrain critical processes in terrestrial planet formation.

## Data Availability Statement

All spectral data used in this study are available in the Open Science Foundation repository https://doi.org/10.17605/OSF.IO/Z6PHN. Spectral data from the NASA RELAB Facility at Brown University are available at https://sites.brown.edu/relab/relab-spectral-database/ and spectral data from the University of Winnipeg Planetary Spectrophotometer Facility are available at http://psf.uwinnipeg.ca/Sample_Database/. The reader is referred to those facilities for the most recent versions of the data and associated archiving information.

**Acknowledgments**
This study was funded by NASA Grant NNM16AA09C. The are no known conflicts of interest for any of the authors. We are extremely grateful to Dr. Laurence Garvie, the ASU Buseck Center for Meteorite Studies, Dr. Timothy McCoy, and the Smithsonian Institution for providing the samples used in this study. We thank Dr. Juan Sanchez and collaborators for sharing spectral data of (16) Psyche. We are grateful to the NASA RELAB Facility at Brown University and the Planetary Spectroscopy Facility at the University of Winnipeg for publicly sharing spectral data. We are extremely grateful to Drs. Richard Binzel, Saverio Cambioni, Vishnu Reddy, and one other anonymous reviewer for improving the clarity of this manuscript.

## References

Adams, J. B. (1974). Visible and near-infrared diffuse reflectance spectra of pyroxenes as applied to remote sensing of solid objects in the solar system. *Journal of Geophysical Research*, *79*(32), 4829–4836. https://doi.org/10.1029/jb079i032p04829

Asphaug, E. (2010). Similar-sized collisions and the diversity of planets. *Geochemistry*, *70*(3), 199–219. https://doi.org/10.1016/j.chemer.2010.01.004

Asphaug, E., & Reufer, A. (2014). Mercury and other iron-rich planetary bodies as relics of inefficient accretion. *Nature Geoscience*, *7*(8), 564–568. https://doi.org/10.1038/ngeo2189

Avdellidou, C., Delbo, M., & Fienga, A. (2018). Exogenous origin of hydration on asteroid (16) Psyche: The role of hydrated asteroid families. *Monthly Notices of the Royal Astronomical Society*, *475*(3), 3419–3428. https://doi.org/10.1093/mnras/sty017

Becker, T. M., Cunningham, N., Molyneux, P., Roth, L., Feaga, L. M., Retherford, K. D., et al. (2020). HST UV observations of asteroid (16) Psyche. *The Planetary Science Journal*, *1*(3), 53. https://doi.org/10.3847/psj/abb67e

Bell, J. F., III, Elkins-Tanton, L. T., Polanskey, C. A., Ravine, M. A., Caplinger, M. A., Asphaug, E., et al. (2016). The Psyche multispectral imager investigation: Characterizing the geology, topography, and compositional properties of a metallic world (Vol. *47*, p. 1366).

Bell, J. F., III, Maki, J. N., Mehall, G. L., Ravine, M. A., Caplinger, M. A., Bailey, Z. J., et al. (2021). The Mars 2020 perseverance rover mast camera zoom (Mastcam-Z) multispectral, stereoscopic imaging investigation. *Space Science Reviews*, *217*(1), 1–40. https://doi.org/10.1007/s11214-020-00755-x

Bercovici, H. L. (2020). *The effect of bulk composition on the sulfur content of cores* (Master's thesis). Arizona State University.

Berger, E. L., Keller, L. P., & Lauretta, D. S. (2015). An experimental study of the formation of cubanite ($CuFe_2S_3$) in primitive meteorites. *Meteoritics & Planetary Science*, *50*(1), 1–14. https://doi.org/10.1111/maps.12399

Berger, E. L., Zega, T. J., Keller, L. P., & Lauretta, D. S. (2011). Evidence for aqueous activity on comet 81P/Wild 2 from sulfide mineral assemblages in Stardust samples and CI chondrites. *Geochimica et Cosmochimica Acta*, *75*(12), 3501–3513. https://doi.org/10.1016/j.gca.2011.03.026

Binzel, R. P., Bus, S. J., Xu, S., Sunshine, J., Burbine, T. H., Neely, A. W., & Brown, R. W. (1995). Rotationally resolved spectra of asteroid 16 Psyche. *Icarus*, *117*(2), 443–445. https://doi.org/10.1006/icar.1995.1170

Britt, D. T., & Pieters, C. M. (1988). Bidirectional reflectance properties of iron-nickel meteorites. In *Lunar and Planetary Science Conference Proceedings* (Vol. 18, pp. 503–512).

Brownlee, D. (2014). The Stardust mission: Analyzing samples from the edge of the solar system. *Annual Review of Earth and Planetary Sciences*, *42*, 179–205. https://doi.org/10.1146/annurev-earth-050212-124203

Burbine, T. H., Buchanan, P. C., & Binzel, R. P. (2007). Deriving formulas from HED spectra for determining the pyroxene mineralogy of Vesta and Vestoids. In *Lunar and Planetary Science Conference* (Vol. 38, p. 2117).

Burbine, T. H., Greenwood, R. C., Buchanan, P. C., Franchi, I. A., & Smith, C. L. (2007). Reflectance spectra of mesosiderites: Implications for asteroid 4 Vesta. In *Lunar and Planetary Science Conference* (Vol. 38, p. 2119).

Burbine, T. H., McCoy, T. J., Nittler, L. R., Benedix, G. K., Cloutis, E. A., & Dickinson, T. L. (2002). Spectra of extremely reduced assemblages: Implications for Mercury. *Meteoritics & Planetary Science*, *37*(9), 1233–1244. https://doi.org/10.1111/j.1945-5100.2002.tb00892.x

Burgess, K. D., & Stroud, R. M. (2021). Exogenous copper sulfide in returned asteroid Itokawa regolith grains are likely relicts of prior impacting body. *Communications Earth & Environment*, *2*(1), 1–6. https://doi.org/10.1038/s43247-021-00187-7

Bus, S. J., & Binzel, R. P. (2002). Phase II of the small main-belt asteroid spectroscopic survey: The observations. *Icarus*, *158*(1), 106–145. https://doi.org/10.1006/icar.2002.6857

Cambioni, S., de Kleer, K., & Shepard, M. (2022). The heterogeneous surface of asteroid (16) Psyche. *Journal of Geophysical Research: Planets*, *127*(6), e2021JE007091. https://doi.org/10.1029/2021je007091

Cantillo, D. C., Reddy, V., Sharkey, B. N., Pearson, N. A., Sanchez, J. A., Izawa, M. R., et al. (2021). Constraining the regolith composition of asteroid (16) Psyche via laboratory visible near-infrared spectroscopy. *The Planetary Science Journal*, *2*(3), 95. https://doi.org/10.3847/psj/abf63b

Chabot, N. L. (2004). Sulfur contents of the parental metallic cores of magmatic iron meteorites. *Geochimica et Cosmochimica Acta*, *68*(17), 3607–3618. https://doi.org/10.1016/j.gca.2004.03.023

Clark, R. N., & Roush, T. L. (1984). Reflectance spectroscopy: Quantitative analysis techniques for remote sensing applications. *Journal of Geophysical Research*, *89*(B7), 6329–6340. https://doi.org/10.1029/jb089ib07p06329

Cloutis, E. A., & Gaffey, M. J. (1991). Pyroxene spectroscopy revisited: Spectral-compositional correlations and relationship to geothermometry. *Journal of Geophysical Research*, *96*(E5), 22809–22826. https://doi.org/10.1029/91je02512

Cloutis, E. A., Gaffey, M. J., Smith, D. G., & Lambert, R. S. J. (1990). Reflectance spectra of "featureless" materials and the surface mineralogies of M-and E-class asteroids. *Journal of Geophysical Research*, *95*(B1), 281–293. https://doi.org/10.1029/jb095ib01p00281

Cloutis, E. A., Hardersen, P. S., Bish, D. L., Bailey, D. T., Gaffey, M. J., & Craig, M. A. (2010). Reflectance spectra of iron meteorites: Implications for spectral identification of their parent bodies. *Meteoritics & Planetary Science*, *45*(2), 304–332. https://doi.org/10.1111/j.1945-5100.2010.01033.x

Cloutis, E. A., Hardersen, P. S., Reddy, V., Gaffey, M. J., Bailey, D. T., & Craig, M. A. (2009). Metal-Orthopyroxene and Metal-Olivine Mixtures: Spectral reflectance properties and implications for asteroid spectroscopy. In *Lunar and Planetary Science Conference* (Vol. 40, p. 1332).

Cloutis, E. A., Hiroi, T., Gaffey, M. J., Alexander, C. O. D., & Mann, P. (2011). Spectral reflectance properties of carbonaceous chondrites: 1. CI chondrites. *Icarus*, *212*(1), 180–209. https://doi.org/10.1016/j.icarus.2010.12.009

Cloutis, E. A., Hudon, P., Hiroi, T., & Gaffey, M. J. (2012a). Spectral reflectance properties of carbonaceous chondrites: 3. CR chondrites. *Icarus*, *217*(1), 389–407. https://doi.org/10.1016/j.icarus.2011.11.004

Cloutis, E. A., Hudon, P., Hiroi, T., & Gaffey, M. J. (2012b). Spectral reflectance properties of carbonaceous chondrites 4: Aqueously altered and thermally metamorphosed meteorites. *Icarus*, *220*(2), 586–617. https://doi.org/10.1016/j.icarus.2012.05.018

Cloutis, E. A., Hudon, P., Hiroi, T., & Gaffey, M. J. (2012c). Spectral reflectance properties of carbonaceous chondrites: 7. CK chondrites. *Icarus*, *221*(2), 911–924. https://doi.org/10.1016/j.icarus.2012.09.017

Cloutis, E. A., Hudon, P., Hiroi, T., Gaffey, M. J., & Mann, P. (2011). Spectral reflectance properties of carbonaceous chondrites: 2. CM chondrites. *Icarus*, *216*(1), 309–346. https://doi.org/10.1016/j.icarus.2011.09.009

Cloutis, E. A., Hudon, P., Hiroi, T., Gaffey, M. J., & Mann, P. (2012d). Spectral reflectance properties of carbonaceous chondrites: 8."Other" carbonaceous chondrites: CH, ungrouped, polymict, xenolithic inclusions, and R chondrites. *Icarus*, *221*(2), 984–1001. https://doi.org/10.1016/j.icarus.2012.10.008

Cloutis, E. A., Hudon, P., Hiroi, T., Gaffey, M. J., & Mann, P. (2012e). Spectral reflectance properties of carbonaceous chondrites–5: CO chondrites. *Icarus*, *220*(2), 466–486. https://doi.org/10.1016/j.icarus.2012.05.019

Cloutis, E. A., Hudon, P., Hiroi, T., Gaffey, M. J., Mann, P., & BellIII, J. F. (2012f). Spectral reflectance properties of carbonaceous chondrites: 6. CV chondrites. *Icarus*, *221*(1), 328–358. https://doi.org/10.1016/j.icarus.2012.07.007

Cloutis, E. A., Sanchez, J. A., Reddy, V., Gaffey, M. J., Binzel, R. P., Burbine, T. H., et al. (2015). Olivine–metal mixtures: Spectral reflectance properties and application to asteroid reflectance spectra. *Icarus*, *252*, 39–82. https://doi.org/10.1016/j.icarus.2014.10.003

de Kleer, K., Cambioni, S., & Shepard, M. (2021). The surface of (16) Psyche from thermal emission and polarization mapping. *The Planetary Science Journal*, *2*(4), 149. https://doi.org/10.3847/psj/ac01ec

DeMeo, F. E., Binzel, R. P., Slivan, S. M., & Bus, S. J. (2009). An extension of the Bus asteroid taxonomy into the near-infrared. *Icarus*, *202*(1), 160–180. https://doi.org/10.1016/j.icarus.2009.02.005

Dibb, S., Bell, J. F., III, Elkins-Tanton, L. T., Williams, D. A., Binzel, R. P., & the Psyche Mission Team. (2018). Optimized narrowband visible to near-infrared filters for the Psyche multispectral imager. In *Instrumentation for Planetary Missions 2018*.

Dibb, S. D., Bell, J. F., III, & Garvie, L. A. (2022). Spectral reflectance variations of aubrites, metal-rich meteorites, and sulfides: Implications for exploration of (16) Psyche and other "spectrally featureless" asteroids. *Meteoritics & Planetary Science*, *57*(8), 1570–1588. https://doi.org/10.1111/maps.13891

Dibb, S. D., Bell, J. F., III, & Garvie, L. A. J. (2021). Reflectance spectra of metal-troilite mixtures: Implications for M-/X-Type asteroid exploration. In *Lunar and Planetary Science Conference* (Vol. 52, p. 1543).

Dyar, M. D., Sklute, E. C., Menzies, O. N., Bland, P. A., Lindsley, D., Glotch, T., et al. (2009). Spectroscopic characteristics of synthetic olivine: An integrated multi-wavelength and multi-technique approach. *American Mineralogist*, *94*(7), 883–898. https://doi.org/10.2138/am.2009.3115

Elkins-Tanton, L. T., Asphaug, E., Bell, J., Bercovici, D., Bills, B. G., Binzel, R. P., et al. (2016). Asteroid (16) Psyche: The science of visiting a metal world (Vol. *47*, p. 1903).

Elkins-Tanton, L. T., Asphaug, E., Bell, J. F., Bierson, C. J., Bills, B. G., Bottke, W. F., et al. (2022). Distinguishing the origin of asteroid (16) Psyche. *Space Science Reviews*, *218*(3), 1–38. https://doi.org/10.1007/s11214-022-00880-9

Elkins-Tanton, L. T., Asphaug, E., Bell, J. F., III, Bercovici, H., Bills, B., Binzel, R., et al. (2020). Observations, meteorites, and models: A preflight assessment of the composition and formation of (16) Psyche. *Journal of Geophysical Research: Planets*, *125*(3), e2019JE006296. https://doi.org/10.1029/2019JE006296

Fornasier, S., Clark, B. E., Dotto, E., Migliorini, A., Ockert-Bell, M., & Barucci, M. A. (2010). Spectroscopic survey of M-type asteroids. *Icarus*, *210*(2), 655–673. https://doi.org/10.1016/j.icarus.2010.07.001

Gaffey, M. J., Cloutis, E. A., Kelley, M. S., & Reed, K. L. (2002). Mineralogy of asteroids. In W. F. Bottke, A. Cellino, P. Paolicchi, & R. P. Binzel (Eds.), *Asteroids III* (pp. 183–204). University of Arizona Press. https://doi.org/10.2307/j.ctv1v7zdn4.20

Garvie, L. A., Knauth, L. P., & Morris, M. A. (2017). Sedimentary laminations in the Isheyevo (CH/CBb) carbonaceous chondrite formed by gentle impact-plume sweep-up. *Icarus*, *292*, 36–47. https://doi.org/10.1016/j.icarus.2017.03.021

Goldstein, J. I., Scott, E. R. D., & Chabot, N. L. (2009). Iron meteorites: Crystallization, thermal history, parent bodies, and origin. *Geochemistry*, *69*(4), 293–325. https://doi.org/10.1016/j.chemer.2009.01.002

Goodrich, C. A., Fioretti, A., Zolensky, M., Shaddad, M., Hiroi, T., Young, E., et al. (2018). Compositional and spectral properties of ureilitic regolith from samples of Almahata Sitta. In *AAS/Division for Planetary Sciences Meeting Abstracts* (Vol. 50, pp. 100–108).

Hardersen, P. S., Cloutis, E. A., Reddy, V., Mothé-Diniz, T., & Emery, J. P. (2011). The M-/X-asteroid menagerie: Results of an NIR spectral survey of 45 main-belt asteroids. *Meteoritics & Planetary Science*, *46*(12), 1910–1938. https://doi.org/10.1111/j.1945-5100.2011.01304.x

Hardersen, P. S., Gaffey, M. J., & Abell, P. A. (2005). Near-IR spectral evidence for the presence of iron-poor orthopyroxenes on the surfaces of six M-type asteroids. *Icarus*, *175*(1), 141–158. https://doi.org/10.1016/j.icarus.2004.10.017

Helbert, J., Maturilli, A., & D'Amore, M. (2013). Visible and near-infrared reflectance spectra of thermally processed synthetic sulfides as a potential analog for the hollow forming materials on Mercury. *Earth and Planetary Science Letters*, *369*, 233–238. https://doi.org/10.1016/j.epsl.2013.03.045

Horgan, B. H., Cloutis, E. A., Mann, P., & BellIII, J. F. (2014). Near-infrared spectra of ferrous mineral mixtures and methods for their identification in planetary surface spectra. *Icarus*, *234*, 132–154. https://doi.org/10.1016/j.icarus.2014.02.031

Ivanova, M. A., Kononkova, N. N., Krot, A. N., Greenwood, R. C., Franchi, I. A., Verchovsky, A. B., et al. (2008). The Isheyevo meteorite: Mineralogy, petrology, bulk chemistry, oxygen, nitrogen, carbon isotopic compositions, and $^{40}$Ar-$^{39}$Ar ages. *Meteoritics & Planetary Science*, *43*(5), 915–940. https://doi.org/10.1111/j.1945-5100.2008.tb01090.x

Izawa, M. R. M., King, P. L., Flemming, R. L., Peterson, R. C., & McCausland, P. J. A. (2010). Mineralogical and spectroscopic investigation of enstatite chondrites by X-ray diffraction and infrared reflectance spectroscopy. *Journal of Geophysical Research*, *115*(E7), E07008. https://doi.org/10.1029/2009je003452

Klima, R. L., Pieters, C. M., & Dyar, M. D. (2007). Spectroscopy of synthetic Mg-Fe pyroxenes I: Spin-allowed and spin-forbidden crystal field bands in the visible and near-infrared. *Meteoritics & Planetary Science*, *42*(2), 235–253. https://doi.org/10.1111/j.1945-5100.2007.tb00230.x

Krot, A. N., Ivanova, M. A., & Ulyanov, A. A. (2007). Chondrules in the CB/CH-like carbonaceous chondrite Isheyevo: Evidence for various chondrule-forming mechanisms and multiple chondrule generations. *Geochemistry*, *67*(4), 283–300. https://doi.org/10.1016/j.chemer.2006.04.001

Landsman, Z. A., Emery, J. P., Campins, H., Hanuš, J., Lim, L. F., & Cruikshank, D. P. (2018). Asteroid (16) Psyche: Evidence for a silicate regolith from spitzer space telescope spectroscopy. *Icarus*, *304*, 58–73. https://doi.org/10.1016/j.icarus.2017.11.035

Larson, W. J., & Wertz, J. R. (1999). *Space mission analysis and design*. Microcosm.

Lauretta, D. S., Lodders, K., & Fegley, B. (1997). Experimental simulations of sulfide formation in the solar nebula. *Science*, *277*(5324), 358–360. https://doi.org/10.1126/science.277.5324.358

Matter, A., Delbo, M., Carry, B., & Ligori, S. (2013). Evidence of a metal-rich surface for the Asteroid (16) Psyche from interferometric observations in the thermal infrared. *Icarus*, *226*(1), 419–427. https://doi.org/10.1016/j.icarus.2013.06.004

McCoy, T. J., Keil, K., Bogard, D. D., Garrison, D. H., Casanova, I., Lindstrom, M. M., et al. (1995). Origin and history of impact-melt rocks of enstatite chondrite parentage. *Geochimica et Cosmochimica Acta*, *59*(1), 161–175. https://doi.org/10.1016/0016-7037(94)00231-a

McSween, H. Y., Jr. (1992). Redox effects in ordinary chondrites and implications for asteroid spectrophotometry. *Icarus*, *95*(2), 239–243. https://doi.org/10.1016/0019-1035(92)90040-e

Mittlefehldt, D. W., McCoy, T. J., Goodrich, C. A., & Kracher, A. (1998). Non-chondritic meteorites from asteroidal bodies. *Planetary materials*, 523–718. https://doi.org/10.1515/9781501508806-019

Morris, M. A., Garvie, L. A., & Knauth, L. P. (2015). New insight into the solar system's transition disk phase provided by the metal-rich carbonaceous chondrite Isheyevo. *The Astrophysical Journal Letters*, *801*(2), L22. https://doi.org/10.1088/2041-8205/801/2/l22

Nedelcu, D. A., Birlan, M., Vernazza, P., Descamps, P., Binzel, R. P., Colas, F., et al. (2007). Near infra-red spectroscopy of the asteroid 21 Lutetia-II. Rotationally resolved spectroscopy of the surface. *Astronomy & Astrophysics*, *470*(3), 1157–1164. https://doi.org/10.1051/0004-6361:20066944

Ockert-Bell, M. E., Clark, B. E., Shepard, M. K., Isaacs, R. A., Cloutis, E. A., Fornasier, S., & Bus, S. J. (2010). The composition of M-type asteroids: Synthesis of spectroscopic and radar observations. *Icarus*, *210*(2), 674–692. https://doi.org/10.1016/j.icarus.2010.08.002

Ockert-Bell, M. E., Clark, B. E., Shepard, M. K., Rivkin, A. S., Binzel, R. P., Thomas, C. A., et al. (2008). Observations of X/M asteroids across multiple wavelengths. *Icarus*, *195*(1), 206–219. https://doi.org/10.1016/j.icarus.2007.11.006

Olsen, E. J., Bunch, T. E., Jarosewich, E., Noonan, A. F., & Huss, G. I. (1977). Happy Canyon: A new type of enstatite achondrite. *Meteoritics*, *12*(2), 109–124. https://doi.org/10.1111/j.1945-5100.1977.tb00336.x

Pirard, E., Bernhardt, H. J., Catalina Hernández, J. C., Brea, C., Segundo, F., & Castroviejo Bolibar, R. (2008). *From spectrophotometry to multispectral imaging of ore minerals in visible and near infrared (VNIR) microscopy*. Australasian Institute of Mining and Metallurgy.

Reddy, V., Le Corre, L., O'Brien, D. P., Nathues, A., Cloutis, E. A., Durda, D. D., et al. (2012). Delivery of dark material to Vesta via carbonaceous chondritic impacts. *Icarus*, *221*(2), 544–559. https://doi.org/10.1016/j.icarus.2012.08.011

Rubin, A. E. (1997). Mineralogy of meteorite groups. *Meteoritics & Planetary Science*, *32*(2), 231–247. https://doi.org/10.1111/j.1945-5100.1997.tb01262.x

Rubin, A. E., & Ma, C. (2017). Meteoritic minerals and their origins. *Geochemistry*, *77*(3), 325–385. https://doi.org/10.1016/j.chemer.2017.01.005

Sanchez, J. A., Reddy, V., Shepard, M. K., Thomas, C., Cloutis, E. A., Takir, D., et al. (2017). Detection of rotational spectral variation on the M-type asteroid (16) Psyche. *The Astronomical Journal*, *153*(1), 29.

Sarid, G., Stewart, S. T., & Leinhardt, Z. M. (2015). Erosive hit-and-run impact events: Debris unbound. *Proceedings of the International Astronomical Union*, *10*(S318), 9–15. https://doi.org/10.1017/s1743921315009679

Schrader, D. L., Davidson, J., & McCoy, T. J. (2016). Widespread evidence for high-temperature formation of pentlandite in chondrites. *Geochimica et Cosmochimica Acta*, *189*, 359–376. https://doi.org/10.1016/j.gca.2016.06.012

Scott, E. R. D., & Krot, A. N. (2003). Chondrites and their components. *Treatise on Geochemistry*, *1*, 711.

Shepard, M. K., de Kleer, K., Cambioni, S., Taylor, P. A., Virkki, A. K., Rívera-Valentin, E. G., et al. (2021). Asteroid 16 Psyche: Shape, features, and global map. *The Planetary Science Journal*, *2*(4), 125. https://doi.org/10.3847/psj/abfdba

Siltala, L., & Granvik, M. (2021). Mass and density of asteroid (16) Psyche. *The Astrophysical Journal Letters*, *909*(1), L14. https://doi.org/10.3847/2041-8213/abe948

Takir, D., Reddy, V., Sanchez, J. A., Shepard, M. K., & Emery, J. P. (2017). Detection of water and/or hydroxyl on asteroid (16) Psyche. *The Astronomical Journal*, *153*(1), 31.

Ulff-Møller, F. (1998). Effects of liquid immiscibility on trace element fractionation in magmatic iron meteorites: A case study of group IIIAB. *Meteoritics & Planetary Science*, *33*(2), 207–220.

Varatharajan, I., Maturilli, A., Helbert, J., Alemanno, G., & Hiesinger, H. (2019). Spectral behavior of sulfides in simulated daytime surface conditions of Mercury: Supporting past (MESSENGER) and future missions (BepiColombo). *Earth and Planetary Science Letters*, *520*, 127–140. https://doi.org/10.1016/j.epsl.2019.05.020

Vernazza, P., Lamy, P., Groussin, O., Hiroi, T., Jorda, L., King, P. L., et al. (2011). Asteroid (21) Lutetia as a remnant of Earth's precursor planetesimals. *Icarus*, *216*(2), 650–659. https://doi.org/10.1016/j.icarus.2011.09.032

Viikinkoski, M., Vernazza, P., Hanuš, J., Le Coroller, H., Tazhenova, K., Carry, B., et al. (2018). (16) Psyche: A mesosiderite-like asteroid? *Astronomy & Astrophysics*, *619*, L3. https://doi.org/10.1051/0004-6361/201834091

Watters, T. R., & Prinz, M. (1979). Aubrites-Their origin and relationship to enstatite chondrites. In *Proceedings of the 10th Lunar and Planetary Science Conference*.

Wood, B. J., & Strens, R. G. J. (1979). Diffuse reflectance spectra and optical properties of some sulphides and related minerals. *Mineralogical Magazine*, *43*(328), 509–518. https://doi.org/10.1180/minmag.1979.043.328.11

Zellner, B., Tholen, D. J., & Tedesco, E. F. (1985). The eight-color asteroid survey: Results for 589 minor planets. *Icarus*, *61*(3), 355–416. https://doi.org/10.1016/0019-1035(85)90133-2

## References From the Supporting Information

Agee, C. B., Vaci, Z., Ziegler, K., & Spilde, M. N. (2019). Northwest Africa 12273: Unique ungrouped metal-rich chondrite. In *Lunar and Planetary Science Conference* (Vol. 2132, p. 1176).

Bild, R. W., & Wasson, J. T. (1976). The Lodran meteorite and its relationship to the ureilites. *Mineralogical Magazine*, *40*(315), 721–735. https://doi.org/10.1180/minmag.1976.040.315.06

Bouvier, A., Gattacceca, J., Agee, C., Grossman, J., & Metzler, K. (2017). The meteoritical bulletin, no. 104. *Meteoritics & Planetary Science*, *52*(10). 2284–2284. https://doi.org/10.1111/maps.12930

Bowman, L. E., Papike, J. J., & Spilde, M. N. (1996). Modal abundances in diogenites: Insights into phase percentages using electron microprobe techniques. In *Lunar and Planetary Science Conference* (Vol. 27, pp. 147–148).

Bunch, T. E., Keil, K., & Huss, G. I. (1972). The Landes meteorite. *Meteoritics*, 7(1), 31–38. https://doi.org/10.1111/j.1945-5100.1972.tb00421.x

Buseck, P. R. (1977). Pallasite meteorites—Mineralogy, petrology and geochemistry. *Geochimica et Cosmochimica Acta*, *41*(6), 711–740. https://doi.org/10.1016/0016-7037(77)90044-8

Gattacceca, J., Mccubbin, F. M., Bouvier, A., & Grossman, J. (2020). The meteoritical bulletin, No. 107. *Meteoritics & Planetary Science*, *55*(2), 460–462. https://doi.org/10.1111/maps.13440

Hutchison, W. K., Bevan, A. W. R., Easton, A. J., & Agrell, S. O. (1981). Mineral chemistry and genetic relations among H-group chondrites. *Proceedings of the Royal Society of London. A. Mathematical and Physical Sciences*, *374*(1757), 159–178.

Jarosewich, E. (1990). Chemical analyses of meteorites: A compilation of stony and iron meteorite analyses. *Meteoritics*, *25*(4), 323–337. https://doi.org/10.1111/j.1945-5100.1990.tb00717.x

Jenniskens, P., Betlem, H., Betlem, J., Barifaijo, E., Schlüter, T., Hampton, C., et al. (1994). The Mbale meteorite shower. *Meteoritics*, *29*(2), 246–254. https://doi.org/10.1111/j.1945-5100.1994.tb00678.x

Keil, K., & Fredriksson, K. (1963). Electron microprobe analysis of some rare minerals in the Norton County achondrite. *Geochimica et Cosmochimica Acta*, *27*(9), 939–947. https://doi.org/10.1016/0016-7037(63)90103-0

Koch, T. E., Brenker, F. E., Krot, A. N., & Bizzarro, M. (2016). Petrography of Quebrada Chimborazo 001—A new CBa chondrite. In *Lunar and Planetary Science Conference* (Vol. 47, p. 1968).

Mason, B. (1963). Olivine composition in chondrites. *Geochimica et Cosmochimica Acta*, *27*(10), 1011–1023. https://doi.org/10.1016/0016-7037(63)90062-0

Moore, C. B., Lewis, C. F., & Clark, J. (1982). The Penwell meteorite revisited. *Meteoritics*, *17*, 256.

Moore, C. B., Lewis, C. F., & Clark, J. C. (1981). The Penwell stony-iron meteorite. *Meteoritics*, *16*, 361.

Powell, B. N. (1971). Petrology and chemistry of mesosiderites—II. Silicate textures and compositions and metal-silicate relationships. *Geochimica et Cosmochimica Acta*, *35*(1), 5–34.

Reid, A. M., Williams, R. J., & Takeda, H. (1974). Coexisting bronzite and clinobronzite and the thermal evolution of the Steinbach meteorite. *Earth and Planetary Science Letters*, *22*(1), 67–74. https://doi.org/10.1016/0012-821x(74)90065-x

Rubin, A. E., & Scott, W. R. (1997). Abee and related EH chondrite impact-melt breccias. *Geochimica et Cosmochimica Acta*, *61*(2), 425–435. https://doi.org/10.1016/s0016-7037(96)00335-3

Russell, S. S., Zipfel, J., Folco, L., Jones, R., Grady, M. M., McCoy, T., & Grossman, J. N. (2003). The meteoritical bulletin, No. 87, 2003 July. *Meteoritics & Planetary Science*, *38*(S7), A189–A248. https://doi.org/10.1111/j.1945-5100.2003.tb00328.x

Ruzicka, A., Grossman, J., Bouvier, A., & Agee, C. B. (2017). The meteoritical bulletin, No. 103. *Meteoritics & Planetary Science*, *52*(5), 1014–1014. https://doi.org/10.1111/maps.12888

Schaudy, R., Watson, J. T., & Buchwald, V. F. (1972). The chemical classification of iron meteorites. VI. A reinvestigation of irons with Ge concentration lower than 1 ppm. *Icarus*, *17*(1), 174–192. https://doi.org/10.1016/0019-1035(72)90053-x

Scott, E. R., Haack, H., & McCoy, T. J. (1996). Core crystallization and silicate-metal mixing in the parent body of the IVA iron and stony-iron meteorites. *Geochimica et Cosmochimica Acta*, *60*(9), 1615–1631. https://doi.org/10.1016/0016-7037(96)00031-2

Ulff-Møller, F., Choi, B. G., Rubin, A. E., Tran, J., & Wasson, J. T. (1998). Paucity of sulfide in a large slab of Esquel: New perspectives on pallasite formation. *Meteoritics & Planetary Science*, *33*(2), 221–227.

Urey, H. C., & Craig, H. (1953). The composition of the stone meteorites and the origin of the meteorites. *Geochimica et Cosmochimica Acta*, *4*(1–2), 36–82. https://doi.org/10.1016/0016-7037(53)90064-7

Weisberg, M. K., Bunch, T. E., Wittke, J. H., Rumble, D., III, & Ebel, D. S. (2012). Petrology and oxygen isotopes of NWA 5492, a new metal-rich chondrite. *Meteoritics & Planetary Science*, *47*(3), 363–373. https://doi.org/10.1111/j.1945-5100.2012.01340.x

Zipfel, J., Wlotzka, F., & Spettel, B. (1998). Bulk chemistry and mineralogy of a new "unique" metal-rich chondritic breccia, Hammadah al Hamra 237. In *Lunar and Planetary Science Conference* (Vol. 29, p. 1417).